R. & M. No. 2127
(7480 & 8363)
A.R.C. Technical Report



MINISTRY OF SUPPLY

AERONAUTICAL RESEARCH COUNCIL
REPORTS AND MEMORANDA

# Design of Suction Slots

*By*

A. FAGE, F.R.S. and R. F. SARGENT
of the Aerodynamics Division, N.P.L.



LONDON: HIS MAJESTY'S STATIONERY OFFICE
Price 5*s.* 6*d.* net

# Design of Suction Slots

*By*

A. FAGE, F.R.S. and R. F. SARGENT
of the Aerodynamics Division, N.P.L.



*Reports and Memoranda No.* 2127

*February,* 1944

*Summary.*—Part I of this report describes experiments, based on visual observations of flow, made to determine the optimum entry shape of a two-dimensional slot suitable for laminar boundary-layer suction. The optimum entry shape, for a given rate of suction, is defined as that for which the velocity of flow into the entry is the lowest possible when it just flows full and flow separation from the front lip is imminent. An entry shape is specified by the throat width, $w$, the radii of curvature, $r_1$ and $r_2$, of the front and back lips respectively, and the angle $\beta$ between the slot axis and the tangent to the surface in the upstream direction. The observations were made for three values, 0·5, 0·8 and 1·4 of the ratio of the rate at which air is sucked into the slot to the rate of flow in the boundary layer, and for $\beta = 15$, 30, 45, 90 and 135 deg.

The entry flow is not sensitive to $r_2/w$. The optimum value of $r_1/w$ increases with $\beta$ and with the rate of suction. The optimum value of the velocity in an entry throat becomes smaller with an increase in $\beta$. A forward-facing slot, $\beta > 90$ deg., has therefore a lower resistance to entry flow than a backward-facing slot, $\beta < 90$ deg. Graphs for use in the design of an optimum slot entry are given, Figs. 6–8.

Part II describes experiments made for slots on the wall of a straight circular pipe. The experimental technique used is based on pressure and velocity measurements in a slot, just beyond the entry.

The work has been undertaken to obtain

(i) a check, from observations made at higher speeds of laminar flow, on the conclusions in Part I,

(ii) the optimum entry shapes of slots for incompressible turbulent boundary-layer suction,

(iii) information on slot entries suitable for turbulent boundary-layer suction at high speeds and on choke conditions of flow.

The conclusions are :—

(i) The graphs given in Part I can be accepted for higher speeds of laminar flow, Figs. 26 and 28.

(ii) The graphs can also be used for turbulent boundary-layer suction, incompressible flow, Figs. 26 and 28.

(iii) The optimum throat width for compressible turbulent flow and no choke, expressed as a fraction of the boundary-layer thickness, is smaller than that for incompressible flow, Table 5.

(iv) The choke width, $w_c$, is given by $\frac{w_c}{\delta} = \frac{m_c}{m}\frac{U_s}{a}$, where $\delta$ is the boundary-layer thickness, $m_c$ is the rate of mass delivery, $m$ is the rate of mass-flow in the boundary layer, $U_s$ is the velocity just outside the boundary layer at the slot position and $a$ is the sonic velocity for isentropic flow, Table 6.

(v) The choke width is independent of the slot angle, but whilst a forward-facing slot designed, for high-speed flow and a medium rate of delivery, to have an optimum entry width, as defined above, may not choke at a higher rate of delivery, a backward-facing slot is likely to choke, Figs. 27 and 29.

*Introduction.*—Boundary-layer suction is likely to have important applications in the future, particularly on jet-driven low-drag aircraft and in the design of cooling systems. Information will then be needed on the optimum entry shape of two-dimensional slots suitable for boundary-layer suction. The present work, presented in Parts I and II, has been undertaken to obtain such information.

The best entry width of a suction slot, designed for a given rate of delivery, is that for which it just flows full; for a greater width, the air forms its own entry by separating from the front lip of the slot; for a smaller width, the velocity of flow into the slot is greater. In either case, the resistance to flow is greater than for the best entry width. The optimum entry shape for an assigned slot angle and an assigned rate of delivery is that for which the velocity of flow into the entry, when it just flows full and separation from the front lip is imminent, is the lowest possible.

The experiments of Part I were made for slots in the floor of a small wind tunnel and for low speeds, in order to obtain a thick boundary layer which would permit the use of wide slots needed for the purpose of visual observation of flow. In view of the low speed at which these experiments were made it was thought desirable to obtain a check, at much higher speeds, on the conclusions drawn from them. These check experiments are described in Part II. They have been made for laminar boundary layer on the wall of a straight pipe of uniform cross-section. The slots used were too narrow to allow visual observation of flow to be made and a different technique, based on measurements of pressure and velocity in a slot, has been used. In addition to these experiments made for a laminar boundary layer, the investigation described in Part II includes experiments made to obtain information on the design of two-dimensional slots suitable for turbulent boundary-layer suction, for both incompressible and compressible subsonic flow. The experiments made for compressible flow include a consideration of the choke conditions in a slot.

## NOTATION

$r$ radius of cross-section of pipe, Part II.

$x$ axial distance measured from the entry to the straight pipe, Part II.

$y$ distance measured normal to surface.

$r_1$ radius of front lip of slot.

$r_2$ radius of back lip of slot.

$h$ height of surface tube.

$w$ width of slot when flow separation from front lip is imminent, measured normal to axis.

$w_c$ choke width of slot.

$\beta$ slot angle, measured between slot axis and tangent to surface in upstream direction.

$\rho$ density in boundary layer
$R$ density outside boundary layer
$R_a$ density at the sonic velocity
} Compressible Flow, Part II, $\rho$ taken for incompressible flow.

$p$ pressure in pipe and on slot wall, Part II.

$u$ velocity in boundary layer measured parallel to surface.

$U$ velocity just outside boundary layer.

$\bar{u}$ mean velocity of flow in pipe, taken to be $Q/\pi r^2 R_0$ for compressible flow.

$u_e$ velocity calculated from surface tube pressure.

$\bar{u}_s$ mean velocity of flow in slot at minimum section when it just flows full, incompressible flow.

$a$ velocity of sound, isentropic expansion of air from rest.

$\delta$ boundary-layer thickness.

$\delta_1$ displacement thickness of boundary layer in pipe, $\int_0^\delta \left(1 - \frac{\rho u}{RU}\right)\left(1 - \frac{y}{r}\right) dy$.

$\theta$ momentum thickness of boundary layer in pipe, $\int_0^\delta \frac{\rho u}{RU}\left(1 - \frac{u}{U}\right)\left(1 - \frac{y}{r}\right) dy$.

$H$ $= \delta_1/\theta$.

NOTATION (*contd.*)

$\mu_w$ coefficient of viscosity at wall.

$\nu$ kinematic viscosity.

$\Lambda$ $\frac{\delta^2}{\nu}\frac{dU}{dx}$, where $x$ is downstream distance.

$\tau_0$ intensity of skin friction.

$U_\tau$ $\sqrt{(\tau_0/\rho)}$.

$Q$ mass-flow in pipe per sec.

$m$ rate of mass-flow in boundary layer per unit span, Part I.
mass-flow in boundary layer on pipe wall per sec., Part II.

$t$ thickness of surface layer just forward of slot when it is not in operation and for which the rate of mass-flow is equal to that into the slot when it is in operation.

$m_1$ mass-flow into slot per unit span per sec., $\int_0^t \rho u dy$, Part I,
and into pipe slot per sec., $\int_0^t 2\pi(r-y)\,\rho u dy$, Part II.

$m_2$ mass-flow per sec. into slot per unit span, Part I, and into pipe slot, Part II, when separation from the front lip is imminent.

$\gamma$ the ratio of the specific heat at constant pressure to the specific heat at constant volume = 1·403.

$M$ The Mach number outside the boundary layer or at the centre of the pipe $= U/\sqrt{(\gamma p/R)}$, Part II.

Suffix 0 denotes quantities at pipe entry, suffix $s$ at slot position without suction, and suffix $A$ in the atmosphere (Part II).

## PART I

### *Slot Experiments in a Low-speed Tunnel*

1. *Wind Tunnel.*—1.1. The flow into a slot entry was observed in a low-speed tunnel, with vertical glass walls, using the smoke filament technique developed by Preston and Sweeting and described in R. & M. 2023[1]. The slots were cut into the floor of the tunnel, well beyond its entry. A low velocity was selected to obtain a thick laminar boundary layer and to allow the use of a wide slot, to facilitate visual observation.

The tunnel had a faired inlet and a box outlet, Fig. 1. Muslin gauze was stretched over the mouth of the inlet and the entry to the box outlet to steady the flow in the tunnel. Most of the observations were taken in the tunnel fitted with a flat floor and roof. The flow conditions near the roof differ from those for an infinite stream, at the same distance from the floor; but early attempts made to simulate the infinite stream conditions by shaping the roof showed that the flow into a slot entry was not sensibly dependent on the flow near the roof, provided the tunnel height was decreased in the direction of flow, to encourage the tunnel to flow full near the slot position. In any case, the presence of the boundary layer on the roof precludes a close resemblance to the conditions in an infinite stream. The tunnel had a height of 3 in. at the inlet and 2·8 in. at the outlet. The height at the slot position was 2·9 in. The tunnel width was 8 in.

Thin vertical glass partitions, with their leading edges 8 in. forward of the slot position, were inserted between the floor and roof of the tunnel, 1·5 in. from the walls, to obtain a closer approximation to two-dimensional flow than would be possible if a slot extended across the whole width of the tunnel and into the thick boundary layers on the tunnel glass walls. The slots extended between the glass partitions, which were 5 in. apart.

Air was sucked through the tunnel and through a slot by a $\frac{1}{6}$-h.p. blower, the pipe system being so arranged that the total rate of flow upstream of the slot and the rate of flow through the slot could be measured separately. The rate of flow through the slot was measured with a plate orifice, and that through the tunnel by the pressure drop in a pipe, calibrated against a plate orifice.

1.2. Entry flow into slots cut into a curved floor was also observed. The shape of the floor resembled, near the slot, that of a Griffith aerofoil. The thickness of the laminar boundary layer near the slot position in the tunnel was 0·61 in. The same thickness, and the same ratio of boundary-layer thickness to radius of curvature, is obtained at the slot position on the Griffith aerofoil at a Reynolds number $\left(\frac{U_0 C}{\nu}\right)$ of $1{\cdot}4 \times 10^6$. The value of the velocity just outside the boundary layer in the tunnel is 1·9 ft./sec., whereas that for the aerofoil would be 17 ft./sec. Apart, then, from the fact that only a small part of the surface of the Griffith aerofoil was represented in the tunnel, the conditions of flow were not dynamically consistent. Nevertheless, a comparison of the results obtained for slots in the curved floor with those for slots in the flat floor gives useful information on the effect of surface curvature on entry flow. The tunnel for these experiments had a curved roof, and its height was 3 in. at the inlet and 2 in. at the outlet. The height at the slot position was 2 in.

2. *Boundary Layer.*—The velocity profile of the boundary layer at the slot position, flat floor, was obtained from measurements of the temperature elevation of a nickel-chromium wire heated by a current maintained at a constant value. The wire was spot welded at its ends to nickel-chromium prongs. It was kept in tension by springiness in the prongs. The length of the wire was 0·5 in. and its diameter was 0·001 in. The temperature elevation, $T$, of the wire above that in the surrounding stream was measured with a copper-constantan thermo-junction at the middle of the wire. The wire was calibrated in the tunnel just beyond the inlet, the velocity, $U$, at the wire position being determined from a direct measurement of the rate of mass-flow in the tunnel. The relation between $T$ and $U$ was given very closely by $1/T = A + B\sqrt{U}$, where $A$ and $B$ are constants.

Fig. 2 gives the velocity profiles, $u/U$ against $y/\delta$, where $u$ is the velocity at a distance $y$ from the surface, $U$ is the velocity just outside the boundary layer and $\delta$ is the thickness of the layer, measured at the slot position for $m_1 = 0$, $m_1 = 0{\cdot}5m$ and $m_1 = 0{\cdot}8\,m$, where $m_1$ is the rate of mass-flow into a slot and $m$ is the rate of mass-flow in the boundary layer, without suction, per unit span. The value of $\delta$ decreases from 0·67 in. to 0·51 in., and $U$ increases from 1·54 ft./sec. to 1·78 ft./sec., with an increase in $m_1$ from 0 to 0·8 $m$. The value of $\Lambda$, *i.e.* $\frac{\delta^2}{\nu}\frac{dU}{dx}$, for $m_1 = 0$ is 4·6. The Blasius velocity profile, $\Lambda = 0$, for a laminar boundary layer is given in Fig. 2. The measured profile for $m_1 = 0$ resembles this theoretical profile: exact agreement is not to be expected because the values of $\Lambda$ differ. For the Blasius profile, the displacement thickness, $\delta_1$, is $0{\cdot}254\delta$ and $m = 0{\cdot}746\ \rho\ \delta\ U_1$. For the measured profile, $m_1 = 0$, $\delta_1 = 0{\cdot}255\ \delta$ and $m = 0{\cdot}745\ \rho\ \delta\ U$. The values of $\delta$ and $U$ for the boundary layer, $m_1 = 0$, at the slot position on the curved floor were not measured. Estimated values, based on theoretical calculations made for the flat and curved floors and the measurements made for the flat floor, are $\delta = 0{\cdot}61$ in., and $U = 1{\cdot}90$ ft./sec.

3. *Entry Shape.*—Flow observations were made for two-dimensional parallel-sided slots having rounded front and back entry lips. An entry shape is therefore closely specified by the width, $w$, given by the normal distance between the parallel sides of the slot, the angle, $\beta$, between the slot axis and the surface, and the radii of curvature, $r_1$ and $r_2$, of the front and back lips respectively (*see* Fig. 3 (*c*)). The velocity profile in the boundary layer just forward of the slot changes with the rate of delivery $m_1$, but for design purposes it is convenient to express $m_1$ in terms of the known rate of mass-flow, $m$, in the boundary layer without suction.

For a given slot entry, *i.e.* for specified values of $\beta$, $w$, $r_1$ and $r_2$, there is a definite value of $m_1$ for which the entry just flows full. This value will be denoted by $m_2$. For $m_1 > m_2$, the entry continues to flow full. For $m_1 < m_2$, the flow separates from the front lip and the entry does not flow full.

Alternatively, for specified values of $\beta$, $r_1$ and $r_2$ there is a definite value of $w$ for a specified value of $m_2$. For a smaller width and the same rate of delivery, the mean velocity into the entry becomes greater and the resistance to flow increases. For a greater width, the flow separates from the front lip. If the increase in width is small, the width of the stream just beyond the entry throat does not change appreciably, provided that the radius $r_1$ of the solid front lip is near its optimum value, but the resistance to flow is greater because of the energy losses associated with the separation. The best width for a specified rate of delivery and specified values of $\beta$, $r_1$ and $r_2$ is therefore that for which the entry just flows full. The mean velocity across the minimum section of the entry is then a minimum. The best entry shape for a specified value of $\beta$ and a specified rate of delivery is that for which the slot just flows full and $w$, $r_1$ and $r_2$ have the optimum values for which the mean entry velocity has its lowest possible value. The purpose of the present observations is to find the optimum values of $w$, $r_1$ and $r_2$ for specified values of $m_2/m$ and $\beta$. The observations were made for $m_1/m = 0{\cdot}5$, $0{\cdot}8$ and $1{\cdot}4$, and for $\beta = 15$, 30, 45, 90 and 135 deg., slots in the flat surface, and $\beta = 15$ and 30 deg. slots in the curved surface. The entry flow was not very sensitive to the values of $r_2$ taken, for in no case did flow separation from a back lip occur within the entry. Accordingly, only $w$ and $r_1$ were varied.

4. *Flow Observation.*—4.1. The flow in the neighbourhood of a slot entry was made visible by smoke filaments, introduced into the surface layer upstream of the slot. The field of flow was illuminated by a beam of light parallel to the span of the slot, and, for the purpose of record, the shadows cast by the slot and the filaments were traced on a sheet of paper attached to a vertical glass wall of the tunnel. Initially, the value of $m_2/m$ for an entry was measured, and then the path of the stagnation filament impinging on the back lip was recorded. Afterwards, the paths of filaments separating from the front lip, and also the stagnation filaments, for those values $0{\cdot}5$, $0{\cdot}8$ and $1{\cdot}4$ of $m_1/m$ which were smaller than the value of $m_2/m$ were recorded. A typical selection of the records taken are given in Fig. 3, slots in a flat surface, and in Fig. 4, slots in the curved surface. In only a few cases were the values of $w$, $r_1$ and $r_2$ for a slot such that it just happened to flow full, $m_1 = m_2$, for one of the selected values of $m_1/m$. Figs. 3 and 4 show, however, that the shapes of the separated filaments resemble those of the solid front lips, in so far as they have well-defined rounded " lips " and are parallel to the slot wall beyond the entry. Filaments that were close to the wall were accordingly taken to give the shapes of solid front lips of slots which would just flow full for the values of $m_1/m$ for which the filaments were recorded. It would, of course, have been possible by systematically varying $w$ with $r_1$ constant, or $r_1$ with $w$ constant, to obtain values of $r_1$ and $w$ for slots which just flow full for the selected values of $m_1/m$, but this refinement was not necessary, because the values of $r_1$ and $w$ obtained for the slots with a filament " front lip " were consistent with those obtained for slots with a solid front lip. In all, flow observations were made for 31 different entries with solid lips.

4.2. Values of $\beta$, $w$, $r_1$ and $r_2$ for the slot entries and $m_2/m = 0{\cdot}5$, $0{\cdot}8$ and $1{\cdot}4$, are given in Table 1. Table 1 also gives values of $\bar{u}_s/U$ and of $t$, where $\frac{\bar{u}_s}{U} = 0{\cdot}745\,\frac{\delta}{w}\,\frac{m_2}{m}$, $\bar{u}_s$ is the mean velocity in the throat of an entry when it just flows full, and $t$ is the thickness of the surface layer just forward of a slot when it is not in operation and for which the rate of mass-flow is equal to that into the slot when it is in operation.

TABLE 1

*Values of $\beta$, $w$, $r_1$ and $r_2$ for Slot Entries and the Values of $m_2/m$ for which they just Flow Full*

(*a*) *Slots in Flat Surface*

$\delta = 0{\cdot}67$ in., $U = 1{\cdot}54$ ft./sec.
$m = 0{\cdot}745\ \rho\ \delta\ U$, $U\delta/\nu = 540$
} for the condition $m_1 = 0$

| $\beta$ deg. | $w$ in. | $r_1$ in. | $r_2$ in. | $m_2/m$ | $t$ in. | $\bar{u}_s/U$ | $\beta$ deg. | $w$ in. | $r_1$ in. | $r_2$ in. | $m_2/m$ | $t$ in. | $\bar{u}_s/U$ |
|---|---|---|---|---|---|---|---|---|---|---|---|---|---|
| 15 | 0·41 | 0·35 | 4·0 | 1·4 | 0·87 | 1·68 | 90 | 0·58 | 0·40 | 0·4 | 1·4 | 0·87 | 1·19 |
| 15 | 0·48 | 0·37 | 4·0 | 1·4 | 0·87 | 1·44 | 90 | 0·75 | 1·00 | 0·4 | 1·4 | 0·87 | 0·92 |
| 15 | 0·39 | 0·38 | 4·0 | 1·4 | 0·87 | 1·76 | 90 | 0·50 | 0·45 | 0·4 | 0·8 | 0·57 | 0·79 |
| 15 | 0·35 | 0·21 | 4·0 | 0·8 | 0·57 | 1·13 | 90 | 0·57 | 0·81 | 0·4 | 0·8 | 0·57 | 0·69 |
| 15 | 0·36 | 0·21 | 4·0 | 0·8 | 0·57 | 1·10 | 90 | 0·59 | 0·70 | 0·4 | 0·8 | 0·57 | 0·67 |
| 15 | 0·32 | 0·24 | 4·0 | 0·8 | 0·57 | 1·23 | 90 | 0·40 | 0·35 | 0·4 | 0·5 | 0·41 | 0·62 |
| | | | | | | | 90 | 0·47 | 0·54 | 0·4 | 0·5 | 0·41 | 0·53 |
| 30 | 0·385 | 0·19 | 4·0 | 0·8 | 0·57 | 1·02 | 90 | 0·45 | 0·44 | 0·4 | 0·5 | 0·41 | 0·55 |
| 30 | 0·41 | 0·25 | 4·0 | 0·8 | 0·57 | 0·97 | | | | | | | |
| 30 | 0·39 | 0·32 | 4·0 | 0·8 | 0·57 | 1·02 | 135 | 0·60 | 0·80 | 0·125 | 1·4 | 0·87 | 1·15 |
| 30 | 0·43 | 0·27 | 4·0 | 0·8 | 0·57 | 0·92 | 135 | 0·42 | 0·50 | 0·125 | 0·8 | 0·57 | 0·94 |
| 30 | 0·32 | 0·16 | 4·0 | 0·5 | 0·41 | 0·77 | 135 | 0·52 | 1·00 | 0·125 | 0·8 | 0·57 | 0·77 |
| 30 | 0·32 | 0·22 | 4·0 | 0·5 | 0·41 | 0·77 | 135 | 0·44 | 2·00 | 0·125 | 0·8 | 0·57 | 0·89 |
| | | | | | | | 135 | 0·58 | 1·60 | 0·125 | 0·8 | 0·57 | 0·68 |
| 45 | 0·40 | 0·20 | 2·0 | 1·4 | 0·87 | 1·73 | 135 | 0·36 | 0·50 | 0·125 | 0·5 | 0·41 | 0·69 |
| 45 | 0·55 | 0·50 | 2·0 | 1·4 | 0·87 | 1·26 | 135 | 0·40 | 1·80 | 0·125 | 0·5 | 0·41 | 0·61 |
| 45 | 0·57 | 0·37 | 2·0 | 1·4 | 0·87 | 1·22 | 135 | 0·50 | 1·50 | 0·125 | 0·5 | 0·41 | 0·50 |
| 45 | 0·37 | 0·20 | 2·0 | 0·8 | 0·57 | 1·07 | | | | | | | |
| 45 | 0·40 | 0·21 | 2·0 | 0·8 | 0·57 | 0·99 | | | | | | | |
| 45 | 0·46 | 0·33 | 2·0 | 0·8 | 0·57 | 0·86 | | | | | | | |
| 45 | 0·32 | 0·16 | 2·0 | 0·5 | 0·41 | 0·77 | | | | | | | |
| 45 | 0·30 | 0·15 | 2·0 | 0·5 | 0·41 | 0·82 | | | | | | | |
| 45 | 0·33 | 0·17 | 2·0 | 0·5 | 0·41 | 0·74 | | | | | | | |
| 45 | 0·36 | 0·20 | 2·0 | 0·5 | 0·41 | 0·69 | | | | | | | |

(*b*) *Slots in Curved Surface*

$\delta = 0{\cdot}61$ in., $U = 1{\cdot}90$ ft./sec.
$m = 0{\cdot}745\ \rho\ \delta\ U$, $U\delta/\nu = 607$
} for the condition $m_1 = 0$

| $\beta$ deg. | $w$ in. | $r_1$ in. | $m_2/m$ | $t$ in. | $\bar{u}_s/U$ |
|---|---|---|---|---|---|
| 15 | 0·425 | 0·35 | 1·4 | 0·79 | 1·49 |
| 15 | 0·350 | 0·20 | 1·4 | 0·79 | 1·82 |
| 15 | 0·305 | 0·24 | 0·8 | 0·52 | 1·20 |
| 30 | 0·31 | 0·29 | 0·8 | 0·52 | 1·18 |
| 30 | 0·32 | 0·32 | 0·8 | 0·52 | 1·13 |
| 30 | 0·22 | 0·21 | 0·5 | 0·37 | 1·03 |

5. *Results.*—5.1. Fig. 5 gives values of $\bar{u}_s/U$ plotted against $r_1/w$, for constant values of $\beta$ and $m_2/m$. Each curve has an optimum value of $r_1/w$ for which the value of $\bar{u}_s/U$ is a minimum. These optimum values, marked by short vertical lines on the curves, are given in Table 2.

TABLE 2

*Optimum Values of $r_1/w$, $\bar{u}_s/U$ and $w/t$*

| $\beta$ deg. | $m_2/m = 0{\cdot}5$ | | | $m_2/m = 0{\cdot}8$ | | | $m_2/m = 1{\cdot}4$ | | |
|---|---|---|---|---|---|---|---|---|---|
| | $r_1/w$ | $\bar{u}_s/U$ | $w/t$ | $r_1/w$ | $\bar{u}_s/U$ | $w/t$ | $r_1/w$ | $\bar{u}_s/U$ | $w/t$ |
| 15 | — | — | — | 0·64 | 1·12 | 0·62 | 0·72 | 1·45 | 0·55 |
| 30 | 0·57 | 0·72 | 0·84 | 0·66 | 0·97 | 0·72 | — | — | — |
| 45 | 0·62 | 0·64 | 0·95 | 0·71 | 0·86 | 0·81 | 0·78 | 1·14 | 0·70 |
| 90 | 1·15 | 0·52 | 1·16 | 1·19 | 0·68 | 1·02 | 1·25 | 0·92 | 0·87 |
| 135 | 2·70 | 0·50 | 1·21 | 2·80 | 0·69 | 1·01 | 2·90 | 0·90 | 0·89 |

They are plotted against $\beta$ with $m_2/m$ constant, in Fig. 6. The optimum value of $r_1/w$ increases with $\beta$, at first slowly and then more rapidly : it also increases slowly with $m_2/m$, $\beta$ being constant. Fig. 5 shows that the optimum values of $r_1/w$, for $\beta = 15$ and 30 deg., obtained for entries in the curved surface, are consistent with those for the flat surface : the difference in surface curvature has not, therefore, sensibly affected the entry flow.

5.2. The optimum values of $\bar{u}_s/U$ and $w/t$, given in Table 2, are plotted against $\beta$ with $m_2/m$ constant, in Figs. 7 and 8 respectively. The optimum value of $\bar{u}_s/U$, for each value of $m_2/m$, becomes smaller as $\beta$ increases. The entry of a forward-facing slot, $\beta > 90$ deg., has therefore a lower resistance to flow, than that of a backward-facing slot, $\beta < 90$ deg. The optimum value of $\bar{u}_s/U$ for $\beta = 135$ deg. is about 60 per cent. of the value for $\beta = 15$ deg. The optimum value of $\bar{u}_s/U$ with $\beta$ constant, increases with $m_2/m$.

The optimum value of $w/t$ increases with $\beta$, $m_2/m$ constant, and decreases with an increase in $m_2/m$ with $\beta$ constant.

For the purpose of design, the thickness of a two-dimensional laminar boundary layer at the slot position (without suction), can be taken to be that given by $\delta^2 = \frac{48{\cdot}1\nu}{U^{6{\cdot}28}} \int_0^x U^{5{\cdot}28}\, dx$, where $x$ is the distance from the stagnation point to the slot, and the velocity distribution in the boundary layer by $\frac{u}{U} = \left(\frac{12 + \Lambda}{6}\right)\frac{y}{\delta} - \frac{\Lambda}{2}\left(\frac{y}{\delta}\right)^2 - \left(\frac{4 - \Lambda}{2}\right)\left(\frac{y}{\delta}\right)^3 + \left(\frac{6 - \Lambda}{6}\right)\left(\frac{y}{\delta}\right)^4$.

5.3. The dependence of the position of the stagnation point on the back lip on $\beta$ and on the rate of suction is shown in Figs. 3 and 4. No records of the flow beyond a stagnation are given because the tunnel flow in this region is not likely to be typical of the flow in practice. Further, no attempt has been made to find the best angle of divergence of the slot walls beyond the entry throat, because this angle can be determined theoretically when the optimum entry width for a given rate of suction is known.

# PART II

## *Slot Experiments in a Long Pipe*

6. *Slots and Pipes.*—6.1. The experiments were made for slots in the wall of a straight 2·25-in. diameter brass pipe. The slots extended completely around the circumference of a cross-section of the pipe, and the flow through them was two-dimensional. The walls of each slot were parallel. The front and back lips of a slot were formed by circular arcs running tangentially into the slot walls and the pipe surface. The entry shapes tested were (*see* Notation and Figs. 9 and 10)

(i) $\beta =$ 30 deg., $r_1 = 0{\cdot}045$ in., $r_2 = 0{\cdot}43$ in., $w$ variable,
(ii) $\beta =$ 30 deg., $r_1 = 0{\cdot}065$ in., $r_2 = 0{\cdot}43$ in., $w$ variable,
(iii) $\beta =$ 150 deg., $r_1 = 0{\cdot}6$ in., $r_2 = 0{\cdot}065$ in., $w$ variable.

The method of varying the slot width is shown in Fig. 11.

6.2. The experiments for incompressible laminar and turbulent flows were made for slots at 21·5 in., from the pipe inlet, Fig. 11. A long faired intake, enclosed in a large box shield with fine linen gauze stretched over its inlet end, was fitted to the pipe to obtain the steady entry conditions needed for the maintenance of a laminar boundary layer on the pipe wall up to the slot position. The intake had a contraction of 16 to 1 on cross-sectional area. The shape chosen resembled that of curve $\psi = 6000$ in Fig. 7 Ref. 2. The experiments for compressible turbulent flow were made for slots at 9 in. from the pipe inlet, Fig. 13. A short faired intake, enclosed in a box shield, was fitted at the inlet. The contraction ratio of the intake was 2·8 to 1 on area. The flow through each pipe was induced by the flow of compressed air from an annular injection slot well beyond the slot under test, Fig. 14.

7. *Boundary-layer Thickness and Rate of Mass-flow.*—7.1. Two considerations influenced the selection of the length of pipe upstream of the slot tested. The first was that if too great a length were taken, the boundary-layer thickness at the slot position would be too large compared with the pipe radius for the results obtained to be representative of those for two-dimensional flow along a plane surface ; the second was that if too small a length were taken, the slot widths would be too small to obtain satisfactory experimental accuracy. The lengths taken gave a boundary-layer thickness, $\delta \simeq 0{\cdot}2r$, where $r$ is the pipe radius, for the incompressible laminar and the compressible turbulent flows, and $\delta \simeq 0{\cdot}3r$ for the incompressible turbulent flow (*see* Table 7).

7.2. The method of estimating the thickness and the rate of mass-flow in the boundary layer is described in the Appendix. Briefly stated, the method is based on the fact that the distribution of the displacement thickness, $\delta_1$, down a pipe can be determined, for measured distributions of velocity and density just outside the boundary layer, from a solution of the momentum equation of the layer, when values are assigned to $[\delta_1]_0$ and $H$, where $[\delta_1]_0$ is the value of $\delta_1$ at the pipe entry and $H = \delta_1/\theta$. Distributions of $\delta_1$ for an assigned value of $[\delta_1]_0$ can also be determined directly from the relation for continuity of mass-flow in the pipe. A close approximation to the true value of $[\delta_1]_0$ is given by that value for which there is a close fit between the distributions of $\delta_1$ obtained by the two methods. When $[\delta_1]_0$ is known, the value of $\delta_1$ at the slot position is given by the mass-continuity relation. The rate of mass-flow in the boundary layer depends not only on $\delta_1$ but also on the form taken for the velocity profile (*see* relation (A5), p. 15). The form chosen for the incompressible laminar flow was the Blasius type, $\Lambda = 0$. The forms taken for the incompressible and compressible turbulent flows, without suction, were fixed by the calculated values of the intensity of skin friction at the slot position. The results of these calculations are given in Table 7 of the Appendix. The velocity profile in the boundary layer just forward of a slot changes with the rate of delivery $m_1$, but for design purposes it is convenient to express $m_1$ in terms of the calculated rate of mass-flow, $m$, in the layer without suction.

8. *Slot-suction system.*—Fig. 14 gives a diagrammatic sketch of the suction system. For the incompressible-flow experiments, the valve $f$ was closed and the valve $d$ was fully open. The flow from suction slot to pump was then through the settling chamber, $a$, the orifice-plate pipes, $b$, the control valves, $c$, the main valve, $d$, and the small suction chamber, $e$. For the compressible-flow experiments, it was necessary to add the additional capacity of the large suction chamber, $g$, because, otherwise, owing to the low pressure at the slot position and the frictional losses in the system, the mass delivery which could be maintained by the pump for the time required to take readings was only a small fraction of the mass-flow in the boundary layer. The method of operation was first to close valve $d$ and to exhaust the air in the chambers $e$ and $g$ to the lowest possible pressure. The valve $d$ was then opened and slot readings were taken until the rise of pressure in these chambers, with the pump in operation, was too great to allow the required rate of flow through the slot to be maintained. The rate of mass-flow was controlled by the valves $c$ and it was measured by plate orifices in the pipes $b$. The cross-sectional areas of the suction pipes, the plate orifices and the valves $d$ and $f$, when fully open, were sufficiently large to prevent choking in them during the compressible-flow experiments.

9. *Experimental Technique.*—9.1. The technique used in Part I to determine optimum entry shape was based on visual observation of flow. In the present work a different technique was used, based on measurements of pressure and velocity in the slot just beyond the entry, because the narrowness of the slots precluded direct observation of flow.

The optimum entry shape for assigned values of slot angle and rate of delivery is defined in Part I as that shape for which the entry just flows full, that is, for which flow separation from the front lip is imminent, when the width $w$ and the radii of curvature, $r_1$ and $r_2$ of the front and back lips have the optimum values which give the lowest possible mean velocity of flow into the entry.

It was found that the entry flow was not very sensitive to the curvature of the back lip, for in no case did the flow separate from this lip. The optimum entry shape, for assigned values of the rate of delivery and slot angle, could therefore be obtained experimentally by systematic variations of $w$ and $r_1$. Such variations were made in the experiments of Part I, and from the results obtained curves of $w/\omega_{opt}$ against $r_1/r_{1opt}$ can be drawn. Such curves, for $\beta = 30$ and 150 deg., are given in Figs. 15 and 16. The values of $r_1$ of the entries tested in the present experiments were chosen to have the same order of magnitude as those of the optimum values deduced from Part I, and, to reduce the number of tests, it was assumed that the curves of Figs. 15 and 16 and also the optimum values of $r_1/\delta$ measured in the earlier work were directly applicable. It was, therefore, only necessary to measure, for assigned values of the rate of delivery and slot angle, the width of the throat of an entry when separation was imminent, for the optimum width could then be found from this measured width, by applying the appropriate correction for the difference between the actual and optimum values of $r_1$. There was no evidence to show how closely the above assumptions held for the compressible turbulent flows but, as will be seen later in Tables 3 and 4, only small corrections were needed.

9.2. When the slot width is smaller than that for which separation occurs and the flow is incompressible, the pressure drop at a hole in the slot wall tends to be proportional to the square of the mean velocity in the slot, and therefore to $1/w^2$. When the width is greater, and the value of $r_1$ is near the optimum, the width of the separated layer and consequently the pressure drop changes slowly with $w$. A measure of $w$ when separation is imminent can therefore be obtained from pressure readings at a hole in the slot wall plotted against $w$. This method forms the basis of the present work.

9.3. A check on the reliability of this method was obtained for one case, the first one considered, by a comparison of the results which it gave with those obtained from readings taken with a small surface tube of the Stanton type (*see* Fig. 32 for shape of tube) situated on the slot wall of the front lip, just beyond the entry.

The condition for flow separation cannot be obtained directly from the readings of a surface tube, unless it is specially calibrated, because the presence of the tube causes premature local separation. The flow is however not affected by the tube when it is completely immersed in the "dead-air" region between the slot wall and a stream which has separated from the wall upstream of the tube.

The pressure at the mouth of the surface tube then approximates closely to the local static pressure measured at a hole in the slot wall. A surface tube can therefore be used to determine the slot width for which the separated layer just clears the tube. The width of the slot when separation is imminent, without the tube in position, is then determined by subtracting from this measured width the height of the tube above the surface.

9.4. A comparison between results given by the two methods was made for incompressible laminar and turbulent flows into slots belonging to the family $\beta = 30$ deg., $r_1 = 0{\cdot}045$ in. and $r_2 = 0{\cdot}43$ in. For the first method, the pressures at two holes $e$ and $f$ in the slot wall (*see* Fig. 9) were measured against a datum pressure, $p_0$, measured at the pipe inlet. For the second method, the pressure at the mouth of a surface tube, situated in line with hole $e$, but offset around the circumference, was measured against the static pressure at hole $e$ and also at hole $d$.

Figs. 17 and 18 give the pressures measured at the holes $d$ and $e$ plotted against $R_w$, where $R_w$ is the reading of the screw used to adjust the slot width. Initially, these pressures fall sharply with an increase in $R_w$, then progressively more slowly and finally at a linear rate. The value of $R_w$ for which separation is imminent is taken to be that for which the pressure begins to fall at a linear rate. Those values of $R_w$ are marked on the curves by arrows. The values of $w$ are given by $\frac{1}{2}R_w$. Figs. 17 and 18 also give curves of the surface-tube pressures plotted against $R_w$. The values of $R_w$ for which the pressure becomes constant and approximately zero are marked by arrows. The values of $w$ for which separation from the front lip is imminent is given, in inches, by $w = \frac{1}{2}R_w - 0{\cdot}007$, where $0{\cdot}007$ in is the height of the tube above the surface. The pressures measured by the surface tube tended to become unsteady for widths near that for which separation just occurs, but they become much steadier at greater widths. This behaviour is to be expected because the boundary of the separated layer fluctuates in position and the surface tube becomes less and less immersed until the local dead-air region is fully established.

9.5. The values of $w/\delta$, obtained from the values of $R_w$ marked in Figs. 17 and 18 are plotted against $m_2/m$ in Fig. 19, where $m_2$ denotes the value of $m_1$ when separation is imminent. The values of $w/\delta$ deduced from the pressure readings at the two holes $d$ and $e$ are in satisfactory agreement with each other and also with those from the surface-tube readings. There was, therefore, no need to use the surface tube for the other slots which were to be tested later.

9.6. In general, the static pressure readings were sufficiently steady to allow the slot width when separation was imminent to be estimated with reasonably good accuracy, but for one or two cases of incompressible flow the readings were too indefinite for this purpose. Apart from these exceptions, the pressure curves for the other cases of incompressible flow resembled in character those shown in Figs. 17 and 18, and for this reason they are not included. The curves for all the cases of compressible flow are given (*see* Figs. 20 to 23) and on them are marked, by arrows, the values of $w/\delta$ for which separation is considered to be imminent. These curves can be classified in two groups :—

(i) Those for which the pressure falls, with an increase in $w/\delta$, to a minimum value and then remains practically constant over a wide range of $w/\delta$, *e.g.*, the curves in Figs. 20a, 21a, 22 and 23.

(ii) Those for which the pressure falls to a well-defined minimum and then rises, *e.g.*, the curves in Fig. 20b and 21b. For the first class, the values of $w/\delta$ taken were those for which the almost constant pressure was first attained, and for the second group those for which the pressure fell to the minimum value. The values of $w/\delta$ thus obtained for the two groups were consistent with each other. Further, there was not any systematic change in the values with $U_s$, over the range $U_s = 387$ to 713 ft./sec. covered for the compressible flows, so that mean values could be taken for this speed range.

9.7. The measured values of $w/\delta$ for which separation in the entry is imminent are given, for both incompressible and compressible flows, together with other relevant data, in Tables 3 and 4. The optimum values of $w/\delta$, determined from these measured values, in the manner described in §9.1 are also given in these Tables.

TABLE 3

$\beta = 30$ deg.

| Flow | Experimental Values | | | | | | $r_1/r_{1\,opt}$ | $w/w_{opt}$ from Fig. 15 | Optimum Values | | | |
|---|---|---|---|---|---|---|---|---|---|---|---|---|
| | $U_s$ ft./sec. | $\delta$ in. | $r_1$ in. | $r_1/\delta$ | $m_2/m$ | $w/\delta$ | | | $m_2/m$ | $r_1/\delta$ | $w/\delta$ | |
| Laminar. Incompressible. | 46·4 | 0·215 | 0·045 | 0·209 | 1·074 | 0·49 | 0·43 | 0·76 | 1·074 | 0·49 | 0·65 | |
| | | | | | 0·805 | 0·44 | 0·52 | 0·81 | 0·805 | 0·40 | 0·54 | |
| | | | | | 0·537 | 0·41 | 0·68 | 0·90 | 0·537 | 0·31 | 0·46 | |
| | 46·4 | 0·215 | 0·065 | 0·303 | 1·00 | 0·64 | 0·66 | 0·90 | 1·00 | 0·46 | 0·71 | |
| | | | | | 0·75 | 0·59 | 0·80 | 0·97 | 0·75 | 0·38 | 0·61 | |
| Turbulent. Incompressible. | 83·6 | 0·376 | 0·045 | 0·120 | 0·830 | 0·43 | 0·30 | 0·68 | 0·830 | 0·40 | 0·63 | |
| | | | | | 0·553 | 0·39 | 0·38 | 0·73 | 0·553 | 0·32 | 0·54 | |
| | | | | | 0·277 | 0·39 | 0·53 | 0·81 | 0·277 | 0·23 | 0·48 | |
| | 83·6 | 0·376 | 0·065 | 0·173 | 0·75 | 0·44 | 0·46 | 0·77 | 0·75 | 0·38 | 0·57 | |
| | | | | | 0·50 | 0·39 | 0·58 | 0·84 | 0·50 | 0·30 | 0·46 | |
| Turbulent. Compressible. | 387 | 0·252 | 0·045 | 0·179 | 0·25 | 0·24 | 0·81 | 0·97 | 0·25 | 0·22 | 0·25 | 0·24 |
| | 553 | 0·244 | 0·045 | 0·185 | 0·25 | 0·25 | 0·84 | 0·98 | 0·25 | 0·22 | 0·25 | |
| | 713 | 0·237 | 0·045 | 0·190 | 0·25 | 0·23 | 0·86 | 0·99 | 0·25 | 0·22 | 0·23 | |
| | 387 | 0·252 | 0·045 | 0·179 | 0·50 | 0·320 | 0·60 | 0·86 | 0·50 | 0·30 | 0·37 | 0·37 |
| | 553 | 0·244 | 0·045 | 0·185 | 0·50 | 0·320 | 0·62 | 0·87 | 0·50 | 0·30 | 0·37 | |
| | 387 | 0·252 | 0·065 | 0·258 | 0·25 | 0·25 | 1·17 | 0·92 | 0·25 | 0·22 | 0·27 | 0·28 |
| | 553 | 0·244 | 0·065 | 0·266 | 0·25 | 0·27 | 1·21 | 0·89 | 0·25 | 0·22 | 0·30 | |
| | 387 | 0·252 | 0·065 | 0·258 | 0·50 | 0·365 | 0·86 | 0·98 | 0·50 | 0·30 | 0·37 | 0·38 |
| | 553 | 0·244 | 0·065 | 0·266 | 0·50 | 0·385 | 0·89 | 0·99 | 0·50 | 0·30 | 0·39 | |

TABLE 4

$\beta = 150$ deg.

| Flow | Experimental Values | | | | | | $r_1/r_{1\,opt}$ | $w/w_{opt}$ from Fig. 16 | Optimum Values | | |
|---|---|---|---|---|---|---|---|---|---|---|---|
| | $U_s$ ft./sec. | $\delta$ in. | $r_1$ in. | $r_1/\delta$ | $m_2/m$ | $w/\delta$ | | | $m_2/m$ | $r_1/\delta$ | $w/\delta$ |
| Laminar. Incompressible. | 46·4 | 0·215 | 0·60 | 2·8 | 0·25 | 0·60 | 1·3 | 0·98 | 0·25 | 2·1 | 0·61 |
| | | | | | 0·50 | 0·77 | 1·1 | 1·00 | 0·50 | 2·7 | 0·77 |
| | | | | | 0·75 | 0·81 | 0·9 | 1·00 | 0·75 | 3·2 | 0·81 |
| | | | | | 1·00 | 0·95 | $0·7_5$ | 0·98 | 1·00 | 3·8 | 0·97 |
| Turbulent Incompressible. | 83·6 | 0·376 | 0·60 | 1·6 | 0·50 | 0·66 | 0·60 | 0·95 | 0·50 | 2·7 | 0·70 |
| Turbulent. Compressible. | 387 | 0·252 | 0·60 | 2·4 | 0·25 | 0·30 | 1·1 | 1·00 | 0·25 | 2·1 | 0·30 } 0·32 |
| | 553 | 0·244 | 0·60 | $2·4_5$ | 0·25 | 0·31 | $1·1_5$ | 1·00 | 0·25 | 2·1 | 0·31 |
| | 713 | 0·237 | 0·60 | 2·5 | 0·25 | $0·33_5$ | 1·2 | 0·99 | 0·25 | 2·1 | 0·34 |
| | 387 | 0·252 | 0·60 | 2·4 | 0·50 | $0·52_5$ | 0·9 | 1·00 | 0·50 | 2·6 | $0·52_5$ } 0·53 |
| | 553 | 0·244 | 0·60 | $2·4_5$ | 0·50 | 0·53 | 0·9 | 1·00 | 0·50 | 2·6 | 0·53 |

10. *Discussion of Results—Incompressible Flow.*—10.1. The optimum values of $w/\delta$ for both laminar and turbulent incompressible flows are plotted against $m_2/m$ in Fig. 26, $\beta = 30$ deg., and in Fig. 28, $\beta = 150$ deg. Curves of $(w/\delta)_{opt}$ and $(r_1/\delta)_{opt}$ obtained from the curves of $w/t$ and $r_1/w$ in Figs. 8 and 6 are also included.

The values of $(w/\delta)_{opt}$, estimated from the tests made for laminar flow into the slots $\beta = 30$ deg. and $r_1 = 0·045$ in., are about 10 per cent. smaller than those given by the curve obtained from Part I, whilst the values from the tests made for the slots $\beta = 30$ deg. and $r_1 = 0·065$ in. are about 5 per cent. greater (Fig. 26). The values of $(w/\delta)_{opt}$ estimated from the results for the slots $\beta = 150$ deg. lie on the curve from Part I within $\pm 4$ per cent. (Fig. 28). It follows, therefore, that the changes in $(w/\delta)_{opt}$ associated with the change in the technique of measurement and with an increase in $(U\delta/\nu)_{slot}$ from 540 in the earlier tests to 5220 in the present tests are not important and that the design curves given in Figs. 6–8 can be accepted without modification. It will be noted that the optimum widths for $\beta = 150$ deg. are about 45 per cent. greater than those for $\beta = 30$ deg.

10.2. The values of $(w/\delta)_{opt}$ estimated from the tests made for turbulent flow into the slots $\beta = 30$ deg. and $r_1 = 0·045$ in. are about 3 per cent. greater and those from the slots $\beta = 30$ deg. and $r_1 = 0·065$ are about 5 per cent. smaller than the values given by the laminar-flow curve obtained from Part I and given in Fig. 26; whilst the single value obtained for turbulent flow into the slot $\beta = 150$ deg. is about 4 per cent. smaller. It appears, therefore, that the design curves given in Part I can be used not only for incompressible laminar flow but also for incompressible turbulent flow into a slot.

For the design of slots for incompressible two-dimensional turbulent boundary-layer flow, the displacement thickness, $\delta$, at the slot (no suction) can be calculated from relation (A7), p. 17. If the velocity distribution is taken to be $u/U = (y/\delta)^{1/n}$, then $\delta = (n + 1)\,\delta_1$.

10.3. Figs. 24 and 25 give pressures on the walls of the slots $\beta = 30$ deg., $r_1 = 0·045$ in., $r_2 = 0·43$ in., measured for laminar and turbulent flows, plotted against distance measured from the cross-section passing through the hole *f*. The widths of the slots were slightly smaller than those for which separation occurs. The curves show that a uniform pressure across a slot is established a short distance beyond the entry throat. The number of pressures taken for each

slot is not sufficient to establish precisely the position, but it appears to be near the section passing through hole *d*. The curves also show the approximate position of the stagnation point on the back lip and the fall in stagnation pressure with a decrease in $m_1/m$.

*Compressible Turbulent Flow.*—10.4. The values of $(w/\delta)_{opt}$ for compressible turbulent flow (*see* Tables 3 and 4) are plotted against $m_2/m$ in Figs. 27 and 29. Table 5 below gives a direct comparison of these values with those for incompressible turbulent flow, which as shown in §10.3 can be taken to be the same as those given by the curves in Figs. 26 and 28 obtained from Part I for incompressible laminar flow.

TABLE 5

*Values of* $(w/\delta)_{opt}$

| | $\beta = 30$ deg. | | $\beta = 150$ deg. | |
|---|---|---|---|---|
| | $m_2/m =$ | | $m_2/m =$ | |
| | 0·25 | 0·50 | 0·25 | 0·50 |
| Compressible Turbulent Flow .. | 0·26 | 0·37$_5$ | 0·32 | 0·53 |
| Incompressible Turbulent Flow .. | 0·43 | 0·51 | 0·61 | 0·73 |
| Ratio .. .. .. | 0·60 | 0·74 | 0·53 | 0·73 |

The values of $(w/\delta)_{opt}$ for compressible flow, $m_2/m = 0{\cdot}25$ and $0{\cdot}50$ are smaller than those for incompressible flow: the ratios range from $0{\cdot}53$ for $\beta = 150$ deg. and $m_2/m = 0{\cdot}25$ to $0{\cdot}74$ for $\beta = 30$ deg. and $m_2/m = 0{\cdot}50$. Measurements of $(w/\delta)_{opt}$ for $m_2/m > 0{\cdot}5$ are not given for, apart from the fact that pressure readings could not be taken, because the pump was too small to maintain delivery for the time that would be needed to take them, choking conditions in a slot arise and have to be considered (*see* §§11.1 to 11·3).

10.5. For the design of slots for compressible two-dimensional turbulent boundary-layer flow, the thickness, $\delta$ of the boundary layer at the slot (no suction) can be estimated by the method given in § A 5.

11. *Choke Experiments.*—11.1. A slot chokes when the outlet pressure is sufficiently far below the inlet pressure to allow overall sonic conditions to be attained in the slot. The rate of mass delivery is then a maximum and independent of the outlet pressure, but the flow pattern beyond the choke depends on this pressure.

The cross-sectional areas of the slots were smaller than those of the circuit pipes, plate orifices and the main and control valves, when opened fully, so that a choke in the system always occurred in a slot. To make choke experiments, the air in the suction chambers *e* and *g*, with the main valve *d* closed, Fig. 14, was first exhausted to the lowest pressure, about 7 in. of mercury, obtainable with the pump. The main and control valves, *d* and *c*, were then opened fully and the speed of flow in the pipe adjusted to a selected value. The pump delivery was, in general, not sufficient to maintain a steady pressure in the suction chambers, but the readings of the plate orifices and the pressure holes in a slot remained steady for a sufficient time to allow them to be recorded, before the pressure in the chambers became too high to maintain the choke. The rate of mass delivery was measured with two plate orifices connected in parallel, except for low rates of delivery when only one orifice was sufficient.

11.2. The rate of mass-flow, $m_c$, for uniform axial velocity at the choke section is $R_a A a$, where $a$ is the sonic velocity for isentropic expansion from the atmospheric condition outside, $A$ is the cross-sectional area at the choke section and $R_a$ is the density at the sonic velocity. The closeness with which the measured values of $m_c/R_a A a$, where $R_a = 0{\cdot}637\ \rho_A$, $a = 0{\cdot}913\ a_A$ and $A$ is taken

to be the throat area of the entry, approach unity gives, therefore, a measure of the closeness with which the actual choking conditions approach the condition of uniform axial velocity in the entry throat.

Fig. 30 gives measured values of $m_c/R_aAa$ plotted against $w/\delta$ for $\beta = 30$ and 150 deg., and $U_s = 387$, 553 and 713 ft./sec. The value of $m_c/R_aAa$ falls with an increase in $U_s$ for a constant value of $w/\delta$. Taking average values for $\beta = 30$ and 150 deg., $m_c/R_aAa$ is about 1 for $U_s = 387$ ft./sec., 0·95 for 553 ft./sec., and 0·85 for 713 ft./sec. Further, for $\beta = 30$ deg. there is a slight tendency for $m_c/R_aAa$ to fall with an increase in $w/\delta$ at a constant value of $U_s$. For $\beta = 150$ deg., $m_c/R_aAa$ is almost constant for each value of $U_s$ when $w/\delta > 0{\cdot}12$. A probable explanation of these results is that for the lower values of $U_s$ and $w/\delta$ the layer sucked into the slot has initially a velocity well below the sonic velocity ultimately attained (except near the slot walls), so that the air tends to accelerate into the slot at a uniform rate and to reach the sonic velocity in a plane cross-section ; on the other hand for the higher values of $U_s$ and $w/\delta$ the velocity of the inner part of the layer is initially much below, whilst that of the outer part is much closer to the sonic velocity, so that the inner part of the layer ultimately attains the sonic velocity later than the outer part and consequently the " surface " of choke is curved. This explanation does not take into account the effect of the curvature of flow into the slot entry, but since the results for $\beta = 30$ deg. have the same general character as those for $\beta = 150$ deg., this effect is probably not of prime importance. The pressures on the slot walls beyond the choke depend on the outlet pressure and, for this reason, are not given. The readings taken showed, however, that the sonic pressure $0{\cdot}528p_A$ was attained either in the entry or just beyond, and that the flow beyond the choke was supersonic when the outlet pressure was sufficiently low.

11.3. Values of $w_c/\delta$, for $\beta = 30$ deg. and constant values of $U_s$, are plotted against $m_c/m$ in Fig. 27. The values of $w_c/\delta$ increase linearly with $m_c/m$, at a rate which increases with $U_s$. The slopes of the curves $w_c/\delta$ against $m_c/m$ are greater than that of the curve $(w/\delta)_{opt}$ against $m_2/m$. The curve of $w_c/\delta$ against $m_c/m$ for the highest speed, $U_s = 713$ ft./sec., cuts the curve of $(w/\delta)_{opt}$ against $m_2/m$ at $m_2/m = m_c/m = 0{\cdot}54$, so that for this rate of delivery the optimum width of the slot when separation is imminent is the same as the width for which choking occurs. It was, unfortunately, not possible to consider, for rates of delivery greater than 0·54 and at high speeds, the flow conditions in a slot for which the width was greater than the choking width, because the pump delivery was not sufficient to maintain a sufficiently low pressure in the suction chambers.

Values of $w_c/\delta$, for $\beta = 150$ deg. and constant values of $U_s$, are plotted against $m_c/m$ in Fig. 29. The value of $w_c/\delta$ increases linearly with $m_c/m$ at a rate which increases with $U_s$, as found for $\beta = 30$ deg. The slopes of the curves of $w_c/\delta$ against $m_c/m$ are, however, smaller than that for $(w/\delta)_{opt}$ against $m_2/m$. The optimum value of $w$, $U_s < 713$ ft./sec., is greater than the choking value.

TABLE 6

| $\beta$ deg. | $U_s$ ft./sec. | $\frac{w_c}{\delta}\frac{m}{m_c}$ | $\frac{w_c}{\delta}\frac{m}{m_c}\frac{a}{U_s}$ |
|---|---|---|---|
| 30 | 713 | 0·73 | 1·04 |
| 30 | 553 | 0·59 } 0·54 | 0·99 |
| | | 0·49 } | |
| 150 | 713 | 0·69 | 0·98 |
| 150 | 553 | 0·52 | 0·96 |
| 150 | 387 | 0·39 | 1·03 |

Table 6 shows that the rate of increase of $w_c/\delta$ with $m_c/m$, *i.e.* $\frac{w_c}{\delta}\frac{m}{m_c}$, for $\beta = 30$ deg. is about the same as that for $\beta = 150$ deg. for the same value of $U_s$, and also that for both values of $\beta$ the choking width is given within $\pm$ 4 per cent. by the relation $\frac{w_c}{\delta}\frac{m}{m_c}\frac{a}{U_s} = 1$.

## APPENDIX

A1. *Estimation of $\delta_1/r$, $\delta/r$ and $m/2\pi r\delta RU$ at Slot Position in Pipe.*—A1.1. The momentum equation of a boundary layer on the wall of a straight cylindrical pipe of uniform cross-section, derived by Young and Winterbottom in R. & M. 2068[3] for the case of a boundary layer which does not extend to the pipe axis is, in the notation given earlier,

$$\theta' = \theta\left[\frac{R'}{R} + (H+2)\frac{U'}{U}\right] = \frac{\tau}{RU^2}, \quad .. \quad .. \quad .. \quad .. \quad .. \quad \text{(A1)}$$

where the dash denotes differentiation with respect to $x$ and $H = \delta_1/\theta$. The momentum thickness, $\theta$, is $\int_0^\delta \frac{\rho u}{RU}\left(1 - \frac{u}{U}\right)\left(1 - \frac{y}{r}\right) dy$, and the displacement thickness, $\delta_1$ is $\int_0^\delta \left(1 - \frac{\rho u}{RU}\right)\left(1 - \frac{y}{r}\right) dy$. Continuity of mass-flow is given by

$$\begin{aligned} Q &= \int_0^\delta 2\pi\rho u\,(r-y)dy + \pi(r-\delta)^2\,RU \\ &= [\pi r^2 - 2\pi r\delta_1]\,RU = [\pi r^2 - 2\pi r\delta_1]_0\,R_0U_0\,, \quad .. \quad .. \quad .. \quad \text{(A2)} \end{aligned}$$

where the suffix 0 denotes quantities at the pipe inlet. For compressible flow, Bernouilli's equation gives

$$\frac{\gamma}{\gamma-1}\frac{p}{\rho} + \frac{u^2}{2} = \frac{\gamma}{\gamma-1}\frac{p}{R} + \frac{U^2}{2} = \frac{\gamma}{\gamma-1}\frac{p_0}{R_0} + \frac{U_0^2}{2} = \frac{\gamma}{\gamma-1}\frac{p_A}{\rho_A}, \quad .. \quad .. \quad \text{(A3)}$$

where $p_A$ and $\rho_A$ are the atmospheric pressure and density respectively. Since the boundary layer does not extend to the pipe axis the adiabatic relation between pressure and density, namely $\frac{p}{R^\gamma} = \frac{p_0}{R_0^\gamma} = \frac{p_A}{\rho_A^\gamma}$, holds on the axis.

For $\gamma = 1{\cdot}4$, we have from relation (A3)

$$\frac{\rho}{R} = 1 - 0{\cdot}2\,M^2\left(1 - \frac{u^2}{U^2}\right), \quad .. \quad .. \quad .. \quad .. \quad .. \quad .. \quad \text{(A4)}$$

where $M = U/a$, and $a$ is the local velocity of sound.

The mass-flow in the boundary layer per second is given by

$$m = \int_0^\delta 2\pi\rho\,u\,(r-y)dy = 2\pi rRU\delta\left[1 - \frac{\delta_1}{\delta} - \frac{\delta}{2r}\right]. \quad .. \quad .. \quad \text{(A5)}$$

The mean pipe velocity, $\bar{u}$, for compressible flow is taken to be $\frac{Q}{\pi r^2 R_0} = \left(1 - 2\frac{\delta_1}{r}\right)_0 U_0$.

For incompressible flow, $\rho = R_0 = R = \rho_A$, $R' = 0$, and the Bernouilli's equation,

$p + \frac{1}{2}\rho U_2 = p_0 + \frac{1}{2}pU_0^2$ holds.

A1.2. Distributions of $\delta_1$ down pipe can be determined by a step-by-step integration of equation (A1) for assigned values of $[\delta_1]_0$ and $H$, when distributions of $U$ and $R$ are known. Distributions of $\delta_1$ can also be determined for these assigned values of $[\delta_1]_0$ and $H$ from the continuity relation (A2).

A close approximation to the true value of $[\delta_1]_0$ is given by that value for which there is a close fit between the two distributions of $\delta_1$. The value of $\delta_1$ at the slot position is then given for this value of $[\delta_1]_0$ by the continuity relation (A2).

A2. *Incompressible Flow, Pipe I.*—The state of flow, laminar or turbulent, in the boundary layer was determined from readings taken with two small surface tubes of the Stanton type, situated at $x = 1{\cdot}78r$ and $16{\cdot}0r$. The readings obtained are plotted in the form $\frac{u_\varepsilon}{U}\frac{\delta}{h}$ against $U$ in Fig. 32, where $u_\varepsilon$ is the velocity calculated from the tube reading taken against the local static pressure and $h$ is the height of the tube above the surface. The initial slow fall in the value of $\frac{u_\varepsilon}{U}\frac{\delta}{h}$ with increase in $U$ indicates that the flow is laminar and the steep rise beyond indicates transition from laminar to turbulent flow. Transition is complete, and turbulent flow is fully established, at the value of $U$ for which $\frac{u_\varepsilon}{U}\frac{\delta}{h}$ attains its maximum value.

The flow at $x = 1{\cdot}78r$ is therefore laminar for speeds below $U = 102$ ft./sec., and at $x = 16r$ below $U = 57$ ft./sec. The maximum value of $U_0$ for which the flow in the pipe remains laminar to the slot position, $x = 19r$, is then 47 ft./sec. The value of $\bar{u}r/\nu$ for the pipe at this speed is 26,500. Fig. 32 also shows that completely developed turbulent flow is established at $x = 1{\cdot}78r$, when $U = 128$ ft./sec. and at $x = 16r$ when $U = 89$ ft./sec. The heights of the surface tubes given in Fig. 32 are approximate : no attempt was made to obtain accurate values because the tubes were used solely to indicate the state of flow and not for the purpose of precise velocity measurement.

A3. *Laminar Boundary Layer. Incompressible Flow, Pipe I.*—A3.1. The boundary-layer equation for a laminar velocity profile, $H = 2{\cdot}58$, can be written in the form

$$\delta_1^2 = \frac{3{\cdot}1\nu}{U^{6{\cdot}28}}\int_0^x U^{5{\cdot}28}\,dx$$

(*see* Ref. 4), where the initial value of $\delta_1$, at $x = 0$, is given by $0{\cdot}70\sqrt{\frac{\nu}{U'}}$. If $x$ is measured from the point where $\delta_1 = (\delta_1)_0$ and $U = U_0$, then

$$\delta_1^2 = \left(\frac{U_0}{U}\right)^{6{\cdot}28}\left[(\delta_1)_0^2 + \frac{3{\cdot}1\nu}{U_0}\int_0^x\left(\frac{U}{U_0}\right)^{5{\cdot}28}dx\right]. \qquad \text{(A6)}$$

A3.2. The distribution of $U/U_0$ measured in pipe $I$ for $U_0 = 48{\cdot}7$ ft./sec. is given in Fig. 31. Comparisons of the distributions of $\delta_1/r$ given by relation (A6) with those given by the mass-continuity relation (A2) for this distribution of $U/U_0$ and three assigned values of $(\delta_1/r)_0$, namely $0{\cdot}0164$, $0{\cdot}0211$ and $0{\cdot}0257$, are shown in Fig. 34. The values of $\bar{u}$ related to these assigned values of $(\delta_1/r)_0$, given by relation (A2), are $47{\cdot}1$, $46{\cdot}65$ and $46{\cdot}2$ ft./sec. respectively. Close agreement between the distributions of $\delta_1/r$ given by the two relations is obtained for $\bar{u} = 46{\cdot}65$ ft./sec. : whereas for $\bar{u} = 47{\cdot}1$ and for $46{\cdot}2$ ft./sec., which are only 1 per cent. greater and 1 per cent. less than $46{\cdot}65$ ft./sec., there are marked and progressive departures with increase in $x/r$. The actual value of $\bar{u}$ for $U_0 = 48{\cdot}7$ ft./sec. was therefore taken to be $46{\cdot}65$ ft./sec. It is estimated from the curves of Fig. 32 that for this value of $U_0$ transition begins at $x = 18{\cdot}4r$, *i.e.* $0{\cdot}6r$ forward of the slot. A lower value of $U_0$, namely $44{\cdot}2$ ft./sec. was therefore selected for the slot experiments to ensure that the flow was laminar at the slot position, $x = 19r$. Values of $\delta_1/r$, $\delta_1/\delta$, $H$ and $m/2\pi r\delta RU$ for the boundary layer at the slot position and $U = 44{\cdot}2$ ft./sec. were estimated for the value of $\delta_1$ obtained for $U_0 = 48{\cdot}7$ ft./sec. on the assumption that the velocity profile, no suction, is the Blasius type for $\Lambda = 0$. These values are given in Table 7.

At the slot, $\delta/r = 0{\cdot}191$, $\delta_1/\delta = 0{\cdot}242$ and $H = 2{\cdot}62$. The value of $\delta_1/\delta$ for a flat plate, $\delta_1/r = 0$, is $0{\cdot}253$, *i.e.* about $4{\cdot}5$ per cent. greater than that for the pipe, whilst $H$ is $2{\cdot}58$, *i.e.* about 2 per cent. smaller.

A4. *Turbulent Boundary Layer. Incompressible Flow, Pipe I.*—A4.1. The slot experiments were made for $U_0 = 79{\cdot}8$ ft./sec. The measured distribution of $U/U_0$ in the pipe is shown in Fig. 31. It can be shown from the curves of Fig. 32 that for $U_0 = 79{\cdot}8$ ft./sec. the flow in the boundary layer is laminar from the inlet to $x = 8{\cdot}4r$ and that it is fully turbulent beyond $x = 15r$. Close agreement between the distributions of $\delta_1/r$ given by relations (A2) and (A6) for the laminar boundary layer from $x = 0$, to $8{\cdot}4r$ was obtained for the assigned value $\bar{u} = 77{\cdot}25$ ft./sec. (*see* Fig. 33). At $x = 15r$, where the turbulent boundary layer is fully established, the value of $\delta_1/r$ given by the mass-continuity relation (2) for $\bar{u} = 77{\cdot}25$ ft./sec. is $0{\cdot}029$.

The momentum equation for the turbulent boundary layer beyond $x = 15r$ was obtained by writing $\tau_0/\rho U^2 = 0{\cdot}00653\ (U\theta/\nu)^{-1/6}$ (Refs. 5 and 6), and $H = 1{\cdot}286$ (*see* later) in equation (A1). This equation then becomes

$$\delta_1' + 3{\cdot}285\,\frac{U'}{U}\,\delta_1 = 0{\cdot}00874\left(\frac{U_1\delta}{\nu}\right)^{-1/6} \quad . \quad . \quad . \quad . \quad . \quad . \quad . \quad . \quad . \quad \text{(A7)}$$

The values of $\delta_1$ obtained from equation (A7) for the initial value $\delta_1/r = 0{\cdot}029$ at $x = 15r$ are plotted in Fig. 33. They are seen to be in close agreement with the values obtained from the mass-continuity relation (A2). The value of $\delta_1/r$ at the slot position is $0{\cdot}038$. The value of $\theta/r = 0{\cdot}0295$.

A4.2. A commonly accepted form for the velocity profile of a turbulent boundary layer is $u/U = 1 + K_1 \log_e (y/\delta)$, where $K_1 = U_\tau/KU$, $K$ can be taken to be $0{\cdot}4$, $U_\tau = \sqrt{(\tau_0/\rho)}$ and $\tau_0$ is the intensity of skin friction. At the slot position, $\theta/r = 0{\cdot}0295$, $U_\tau/U = 0{\cdot}044$ and $K_1 = 0{\cdot}110$. For this velocity profile on a flat plate, $y/r = 0$, we have $H = 1/(1{-}2K_1) = 1{\cdot}282$ and $\delta_1/\delta = K_1 = 0{\cdot}110$ (*see* later). An alternative form for the velocity profile of a turbulent boundary layer is $u/U = (y/\delta)^{1/n}$. For a flat plate, $H = (n + 2)/n$, so that for $H = 1{\cdot}282$ we have $n = 7{\cdot}1$. For $n = 7{\cdot}1$, $\delta_1/\delta = 1/(n + 1) = 0{\cdot}124$, *i.e.* 13 per cent. greater than the value for the logarithmic velocity distribution.

A4.3. To obtain estimates of the values of $\delta/r$, $\delta_1/\delta$ and $m/2\pi r\delta RU$ at the slot position in the pipe, we assume the velocity profile to be $u/U = (y/\delta)^{1/7{\cdot}1}$. For pipe flow, $\dfrac{\delta_1}{\delta} = \dfrac{1}{1+n} - \dfrac{\delta}{2r}\dfrac{1}{(1+2n)}$ and $\dfrac{\theta}{\delta} = \dfrac{n}{(1+n)\,(2+n)} - \dfrac{\delta}{2r}\dfrac{n}{(1+n)\,(1+2n)}$. The values of $\delta/r$, $m/2\pi r\delta RU$ and $H$ calculated for $n = 7{\cdot}1$ and the estimated value $\delta_1/r = 0{\cdot}038$ are given in Table 7.

A5. *Turbulent Boundary Layer. Compressible Flow, Pipe II.*—A5.1. The slot experiments were made for $U_0 = 372$, 527 and 673 ft./sec. The measured distributions of $U/U_0$ and $R/R_0$ are given in Fig. 35. The flow in the boundary layer was turbulent at the pipe inlet for each speed.

To obtain a boundary-layer equation for compressible flow in a form consistent with that for incompressible flow we take

$$\tau_0/\rho U^2 = 0{\cdot}00653\ (U\theta R/\mu_w)^{-1/6}\ .$$

Equation (A1) then becomes

$$\delta_1' + \delta_1\left[\frac{R'}{R} + (H+2)\,\frac{U'}{U}\right] = 0{\cdot}00653\,H\left(\frac{U\delta_1 R}{H\mu_w}\right)^{-1/6} . \quad . \quad . \quad . \quad . \quad . \quad \text{(A8)}$$

The values of $H$ taken for the three speeds were $1{\cdot}311$, $1{\cdot}369$ and $1{\cdot}455$ respectively (*see* later). The values of $(\delta_1/r)_0$ found by trial to give close agreement between the distributions of $\delta_1/r$ determined from equation (A8) with those from the mass-continuity relation (A2) are $0{\cdot}0075$, $0{\cdot}0058$ and $0{\cdot}0076$ respectively (*see* Fig. 35). The values of $\delta_1/r$ at the slot position are $0{\cdot}0242$, $0{\cdot}0227$ and $0{\cdot}0242$ respectively.

A5.2. The values of $\delta_1/\delta$, $H$ and $m/2\pi r\delta RU$ at the slot position were estimated by a method based on that used for incompressible flow. To illustrate the method we take the case for $U_0 = 527$ ft./sec.

For a turbulent boundary layer on a flat plate, compressible flow, and a velocity profile of the form $u/u = 1 + K_1 \log_e (y/\delta)$, where $K_1 = U_\tau/KU$, we have from Ref. 7

$$H = \frac{1}{1-2K_1} \frac{1 + \{0\cdot4 - 1\cdot2K_1 + 1\cdot2K_1^2\} M^2}{1 + \{(-0\cdot8K_1 + 3\cdot6K_1^2 - 4\cdot8K_1^3)/(1-2K_1)\}M^2}$$

and

$$\delta_1/\delta = K_1 + M^2\{0\cdot4K_1 - 1\cdot2K_1^2 + 1\cdot2K_1^3\}.$$

For $U_0 = 527$, $M = 0\cdot511$ at the slot position and the value of $U_\tau/U$ estimated from the relation $(U_\tau/U)^2 = 0\cdot00653\,(U\delta_1 R/H\mu_w)^{-1/6}$ is $0\cdot040$. On the assumption that $K = 0\cdot4$, the incompressible flow value, we get $K_1 = 0\cdot100$, $H = 1\cdot367$ and $\delta_1/\delta = 0\cdot108$.

For a velocity profile $u/U = (y/\delta)^{1/n}$ on a flat plate we have, using the relation $\rho/R = 1 - 0\cdot2\,M^2\{1 - (u^2/U^2)\}$,

$$H = \frac{(2+n)}{n} \frac{\{1 + [0\cdot4n/(3+n)]M^2\}}{\{1 - [(0\cdot8n+2)/(3+n)\,(4+n)]M^2\}}$$

and

$$\frac{\delta_1}{\delta} = \frac{1}{(1+n)} \left\{1 + \frac{0\cdot4n\,M^2)}{3+n}\right\}.$$

For $M = 0\cdot511$, $H = 1\cdot367$ when $n = 8\cdot00$. For $M = 0\cdot511$ and $n = 8\cdot0$, $\delta_1/\delta = 0\cdot1195$, *i.e.* 11 per cent. greater than the value for the logarithmic profile.

A5.3. To obtain estimates of the values of $\delta/r$, $\delta_1/\delta$ and $m/2\pi r\delta RU$ at the slot position, we assume the velocity profile to be $u/U = (y/\delta)^{1/8}$. For pipe flow,

$$\frac{\delta_1}{\delta} = \frac{1}{1+n}\left\{1 + \frac{0\cdot4n\,M^2}{3+n}\right\} - \frac{\delta}{r}\left\{\frac{1}{2(1+2n)} + \frac{0\cdot4\,M^2n}{(1+2n)\,(3+2n)}\right\},$$

and

$$\frac{\theta}{\delta} = \frac{n}{(1+n)(2+n)}\left\{1 - \frac{(0\cdot8n+2)M^2}{(3+n)\,(4+n)}\right\} - \frac{\delta}{2r}\,\frac{n}{(1+n)\,(1+2n)}\left\{1 - \frac{M^2\,(2+1\cdot6n)}{(3+2n)\,(4+2n)}\right\}.$$

The values of $\delta/r$ and $H$ obtained from these relations for $n = 8\cdot0$ and $\delta_1/r = 0\cdot0227$ are $0\cdot201$ and $1\cdot369$ respectively. The value of $m/2\pi r\delta RU$ is $0\cdot787$. Similar calculations were made for the cases $U_0 = 372$ and 673 ft./sec. The results obtained are given in Table 7.

# TABLE 7

| | Inlet Values | | | | | Slot Values | | | | | | | | | | Flat Plate $\delta/r = 0$ | |
|---|---|---|---|---|---|---|---|---|---|---|---|---|---|---|---|---|---|
| | $U_0$ ft./sec. | $\bar{u}$ ft./sec. | $R_0/\rho_A$ | $\delta_1/r$ | $M_0$ | $K_1$ | $n$ | $M$ | $\delta_1/r$ | $U$ ft./sec. | $R/\rho_A$ | $H$ | $\delta_1/\delta$ | $\delta/r$ | $\frac{m}{2\pi r \delta R U}$ | $H$ | $\delta_1/\delta$ |
| Incompressible Flow. Laminar Boundary Layer. Pipe I. | 44·2 | 42·3 | 1 | 0·022 | — | — | — | — | 0·046 | 46·4 | 1 | 2·62 | 0·242 | 0·191 | 0·662 | 2·58 | 0·253 |
| Incompressible Flow. Turbulent Boundary Layer.* Pipe I. | 79·8 | 77·3 | 1 | 0·016 | — | 0·110 | 7·1 | — | 0·0380 | 83·6 | 1 | 1·300 | 0·114 | 0·334 | 0·719 | 1·282 | 0·124 |
| Compressible Flow. Turbulent boundary Layer. Pipe II. | 372 | 368 | 0·946 | 0·0075 | 0·337 | 0·101 | 8·0 | 0·351 | 0·0242 | 387 | 0·941 | 1·311 | 0·108 | 0·224 | 0·780 | 1·307 | 0·115 |
| | 527 | 521 | 0·898 | 0·0058 | 0·487 | 0·100 | 8·0 | 0·511 | 0·0227 (0·0242)† | 553 | 0·887 | 1·369 | 0·113 | 0·201 (0·217)† | 0·787 (0·780)† | 1·367 | 0·120 |
| | 673 | 663 | 0·828 | 0·0076 | 0·628 | 0·098 | 8·3 | 0·666 | 0·0242 | 713 | 0·809 | 1·455 | 0·115 | 0·211 | 0·780 | 1·440 | 0·121 |

* Laminar boundary layer at entry.

( )† These values taken in calculations.

## REFERENCES


| *No.* | *Author* | *Title, etc.* |
|---|---|---|
| 1 | Preston and Sweeting.. .. | An Improved Smoke Generator for use in the Visualisation of Airflow, particularly Boundary-layer Flow at High Reynolds Numbers. R. & M. 2023. October, 1943. |
| 2 | Batchelor and Shaw .. .. | A Consideration of the Design of Wind-tunnel Contractions. Division of Aeronautics, C.S.I.R. Australia, Report A.15, S. & M. 22. September, 1943. A.R.C. 7306. |
| 3 | Young and Winterbottom .. | High-speed Flow in Smooth Cylindrical Pipes of Circular Cross-section. R. & M. 2068. November, 1942. |
| 4 | Young and Winterbottom .. | Note on the Effect of Compressibility on the Profile Drag of Aerofoils in the absence of Shock Waves. R.A.E. Report B.A. 1595. A.R.C. 4667. May, 1940. (To be published.) |
| 5 | Falkner .. .. .. | The Resistance of a Smooth Flat Plate with Turbulent Boundary Layer. *Aircraft Engineering*, Vol. XV. No. 169. March, 1943. |
| 6 | Garner .. .. .. .. | The Development of Turbulent Boundary Layers. R. & M. 2133. June, 1944. |
| 7 | Emerson and Young .. .. | High-speed Flow in slowly Convergent and Divergent Pipes and Channels. Part I—Meridian Profiles for Pipes and Channels with Constant Axial Mach Numbers. R.A.E. Report Aero 1957. A.R.C. 8059. July, 1944. (Unpublished.) |

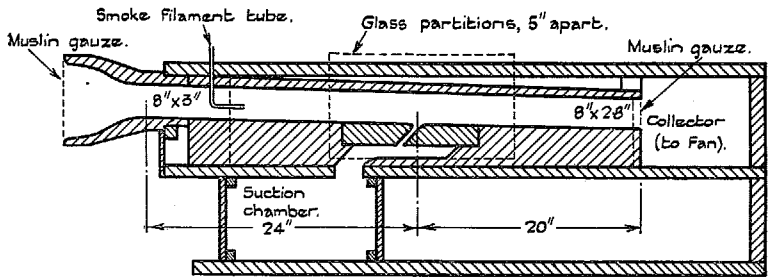


FIG. 1. Median Section of Tunnel.

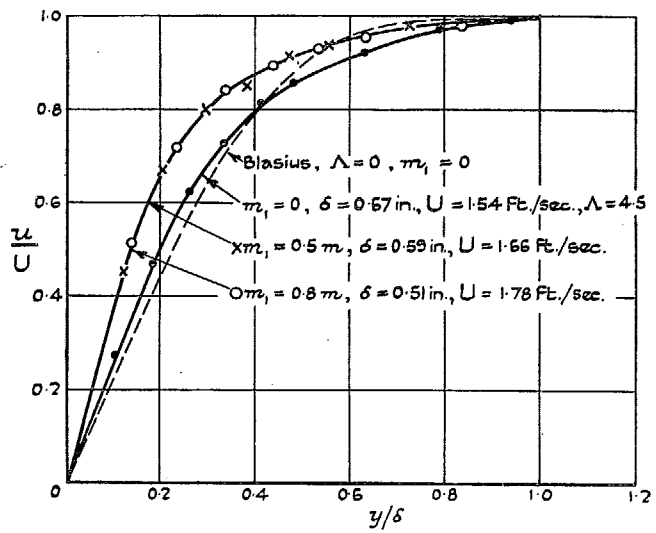


FIG. 2. Velocity Profile of Boundary Layer.

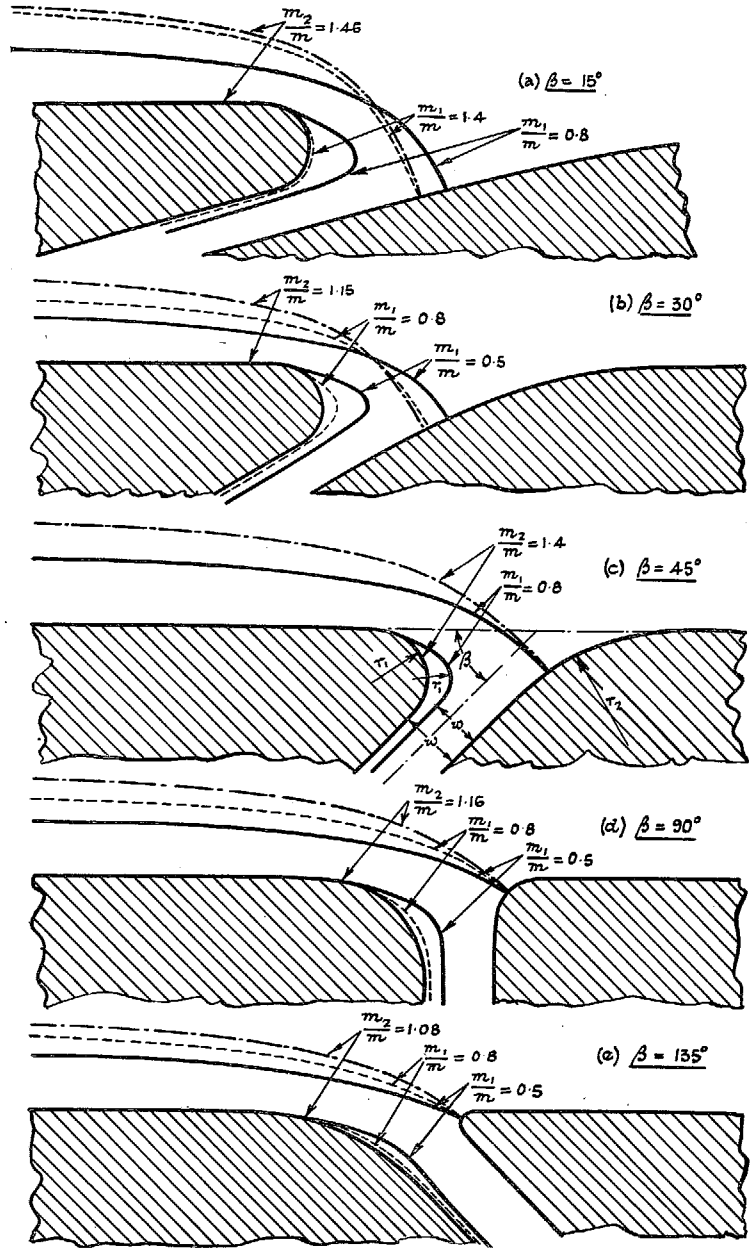


FIG. 3. Flow into Entries of Slots in Flat Surface.

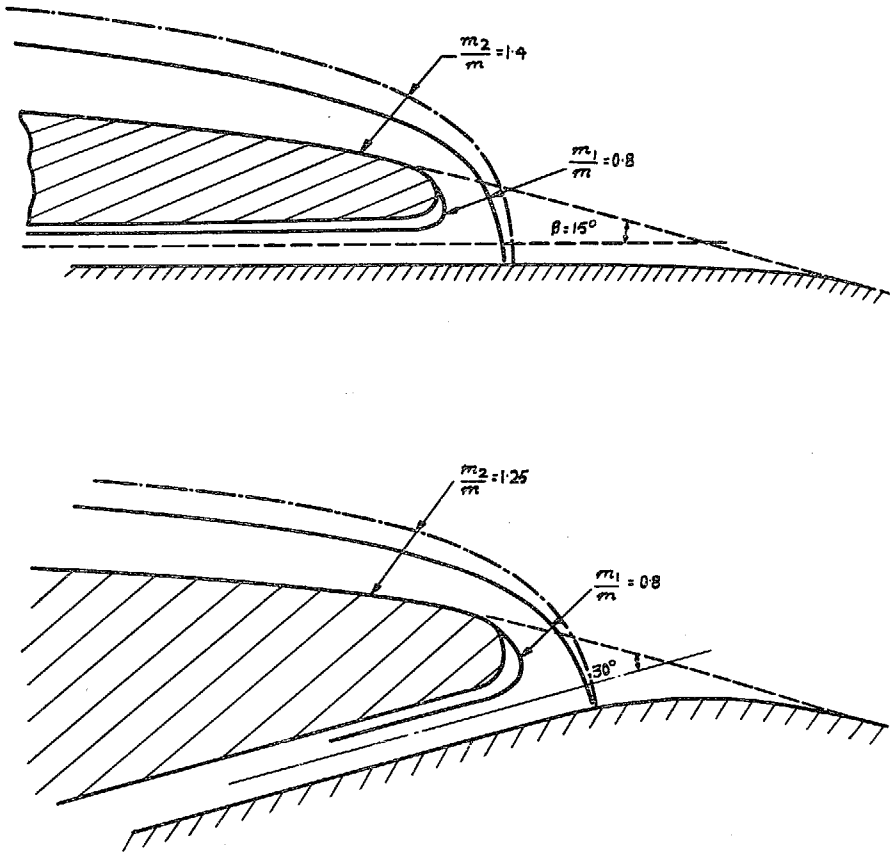


FIG. 4. Flow into Entries of Slots in Curved Surface.

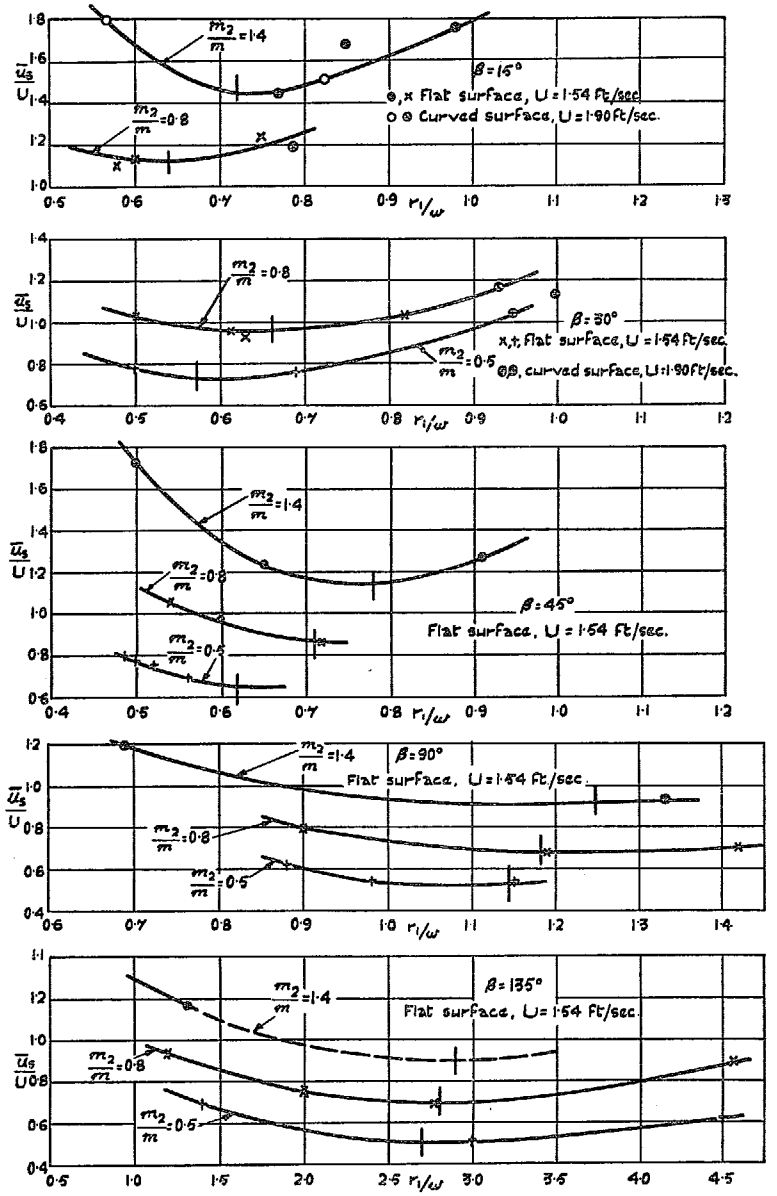


FIG. 5. Variation of Mean Velocity, $\bar{u}_s$, in Slot Entry with Ratio of Radius of Curvature, $r_1$, of Front Lip to Slot Width $w$.

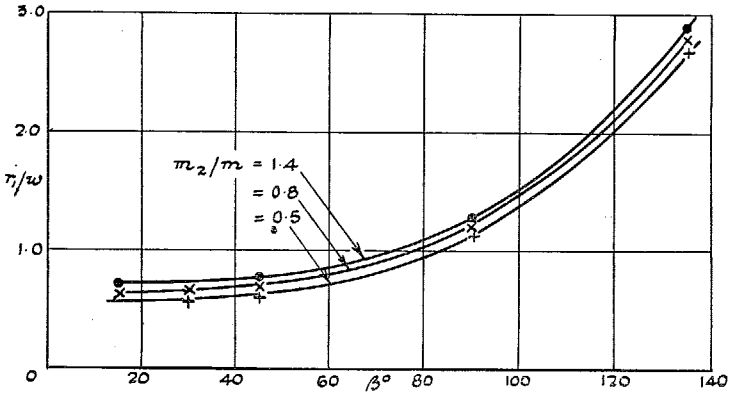


FIG. 6. Variation of Ratio of Optimum Radius of Curvature, $r_1$, of Front Lip to Slot Width, $w$, with Slot Angle, $\beta$.

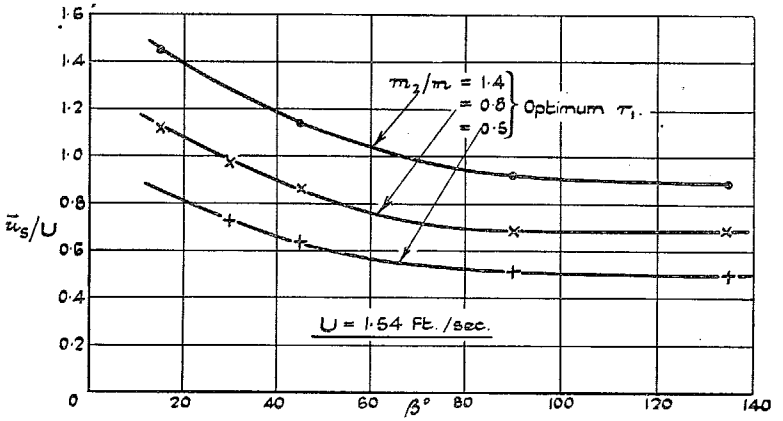


FIG. 7. Variation of Mean Velocity, $\bar{u}_s$, in Slot Entry with Slot Angle, $\beta$.

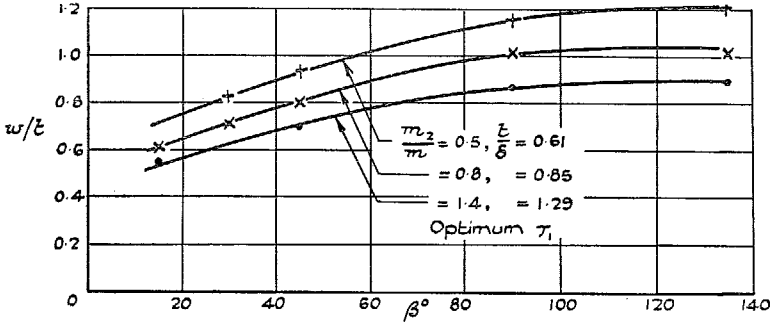


FIG. 8. Variation of Ratio of Slot Width, $w$, to Thickness of Layer Sucked, $t$, with Slot Angle, $\beta$.

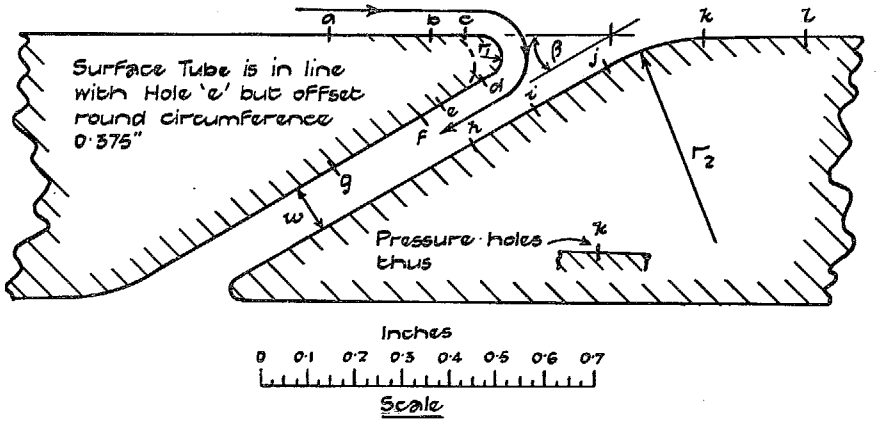


For sketch of a surface tube *see* Fig. 32.

$r_1 = 0{\cdot}045$ in. and $0{\cdot}065$ in.
$r_2 = 0{\cdot}43$ in.
$\beta = 30$ deg.
$w$ is variable.

FIG. 9.

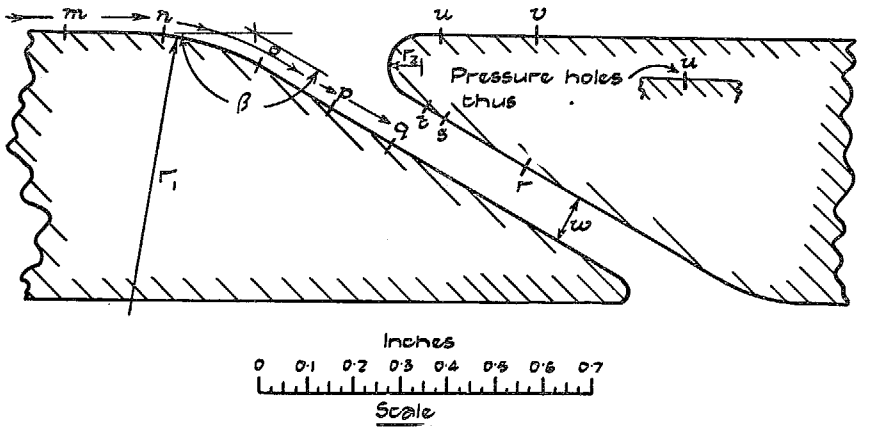


$r_1 = 0{\cdot}6$ in.
$r_2 = 0{\cdot}065$ in.
$\beta = 150$ deg.
$w$ is variable.

FIG. 10.

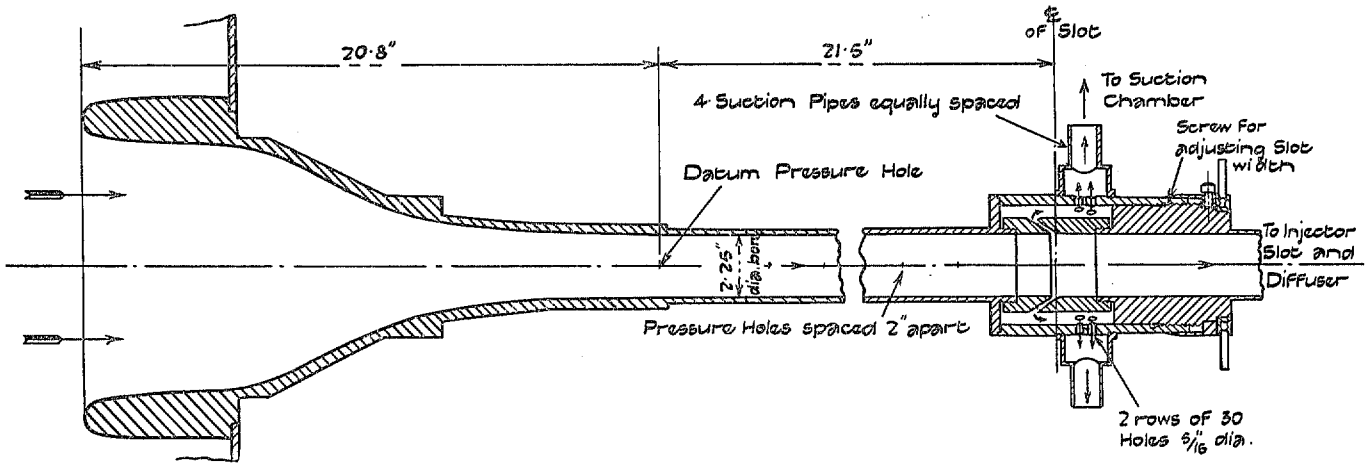


FIG. 11.

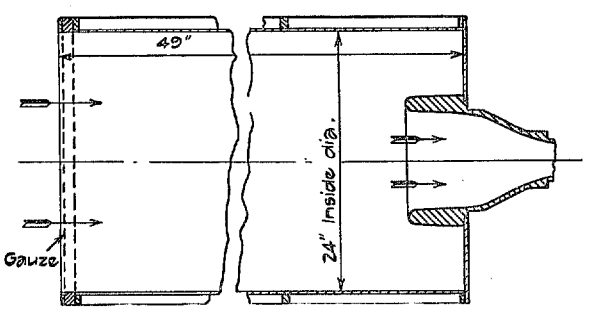


FIG. 12. Box Shield for Intake.

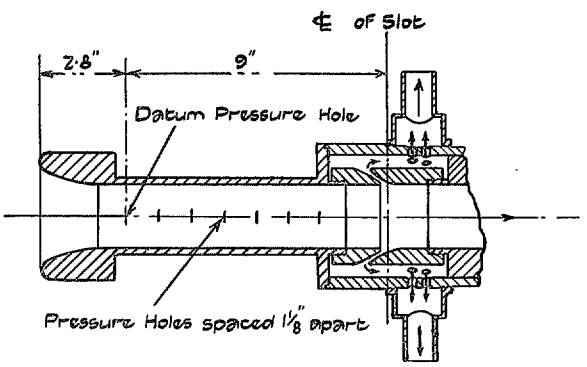


FIG. 13.

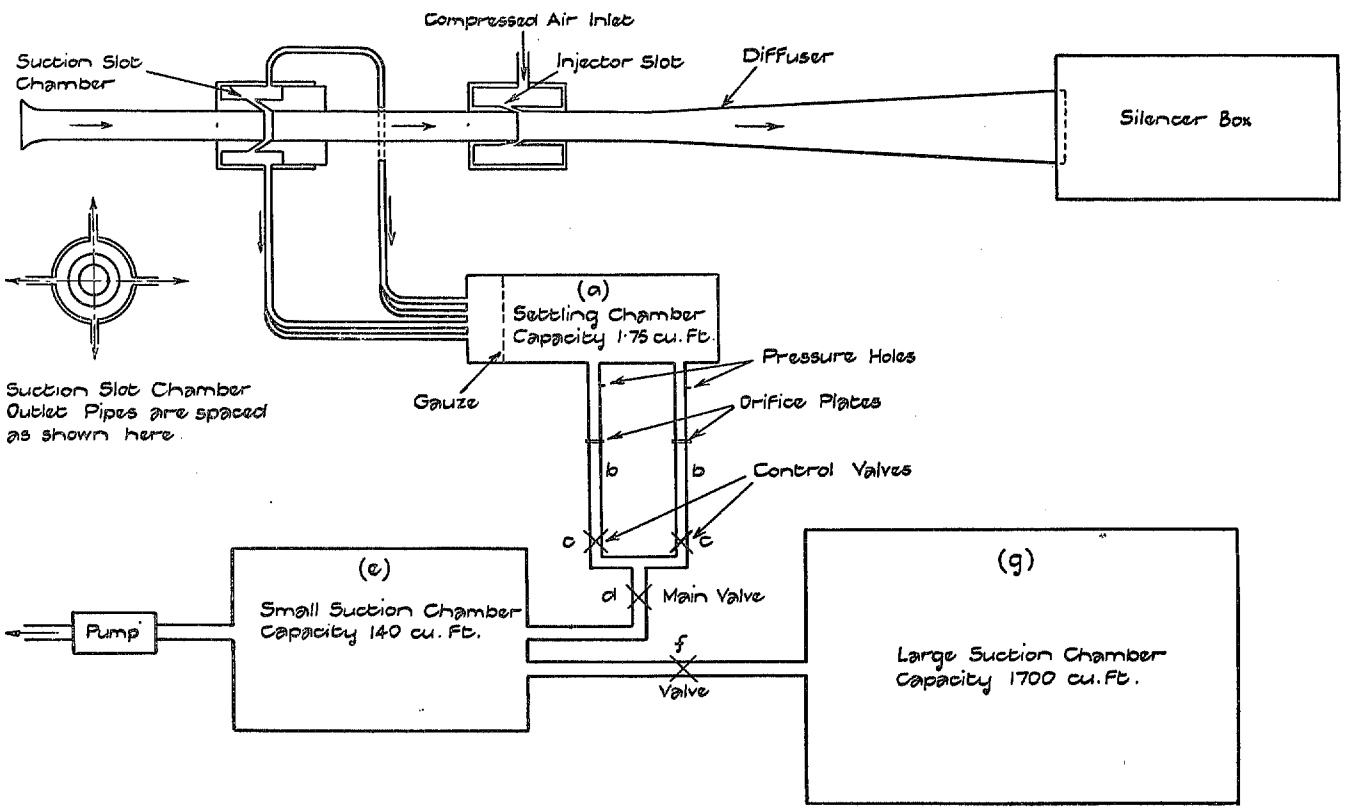


FIG. 14. Diagrammatic Sketch of Suction System.

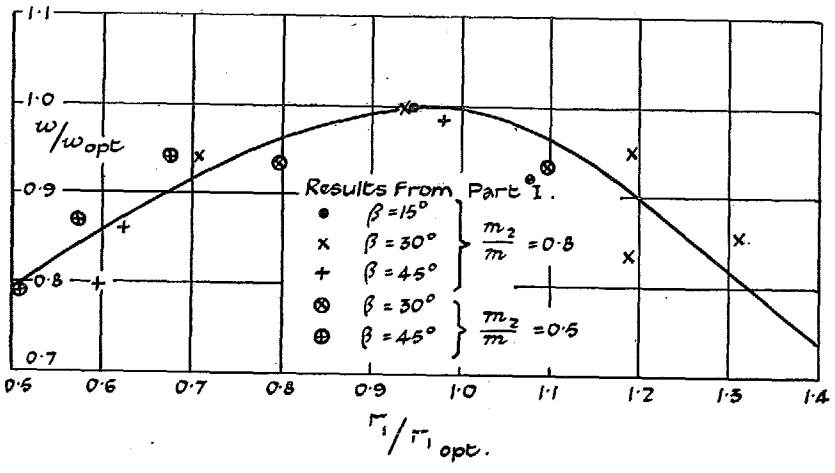


FIG. 15.

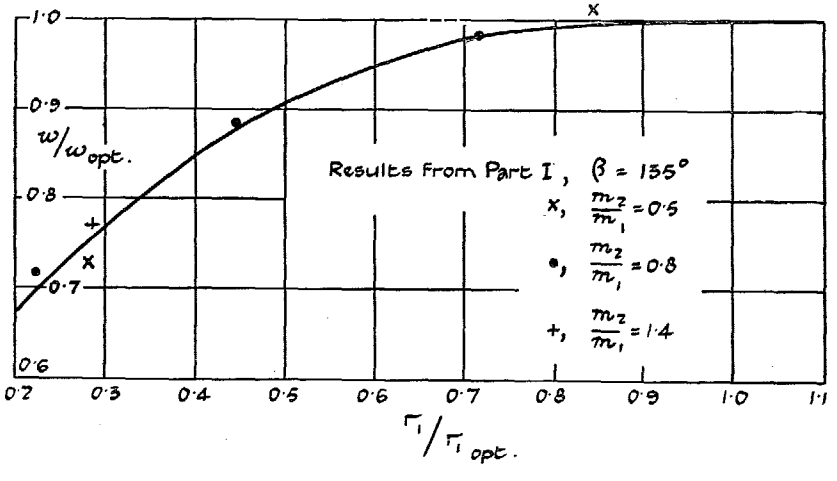


FIG. 16.

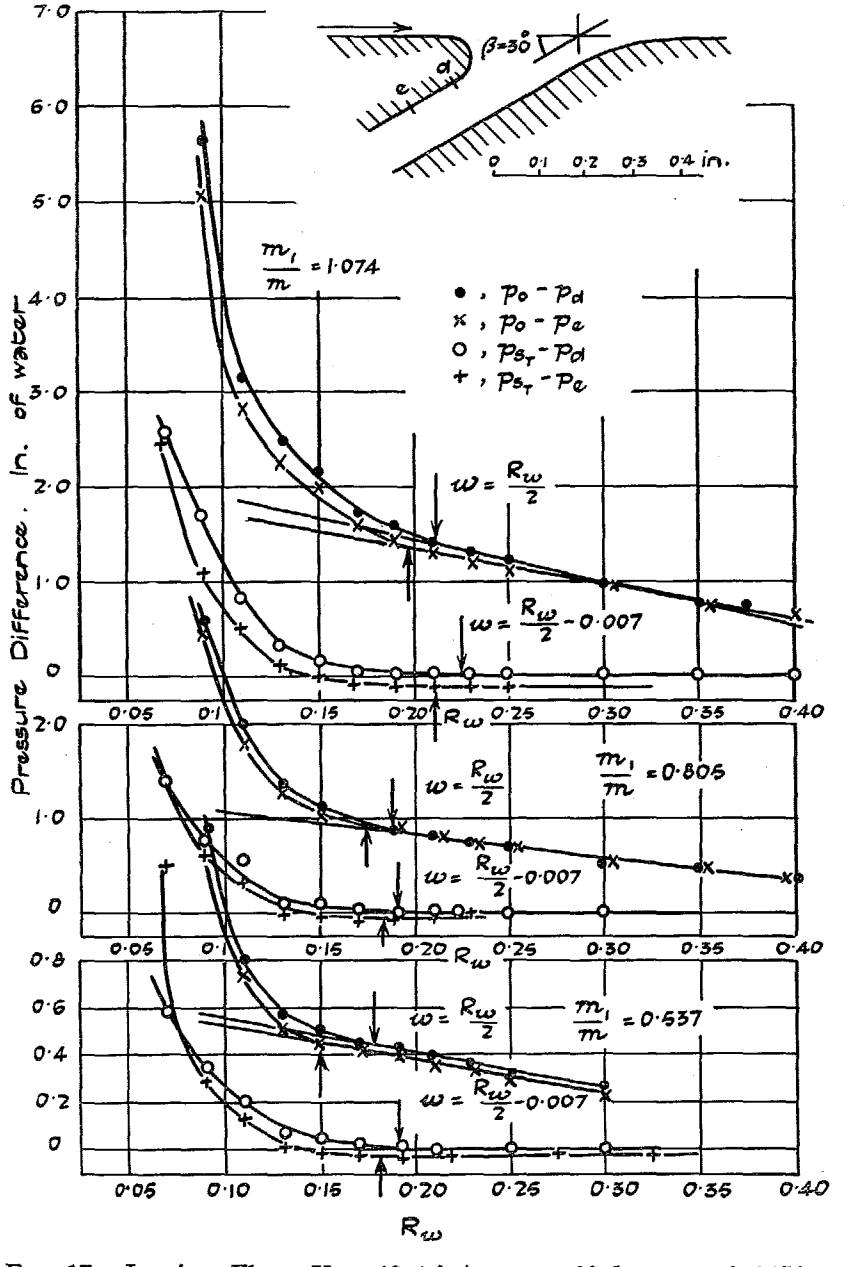


FIG. 17. Laminar Flow. $U_s = 46{\cdot}4$ ft./sec. $\beta = 30$ deg., $r_1 = 0{\cdot}045$ in.

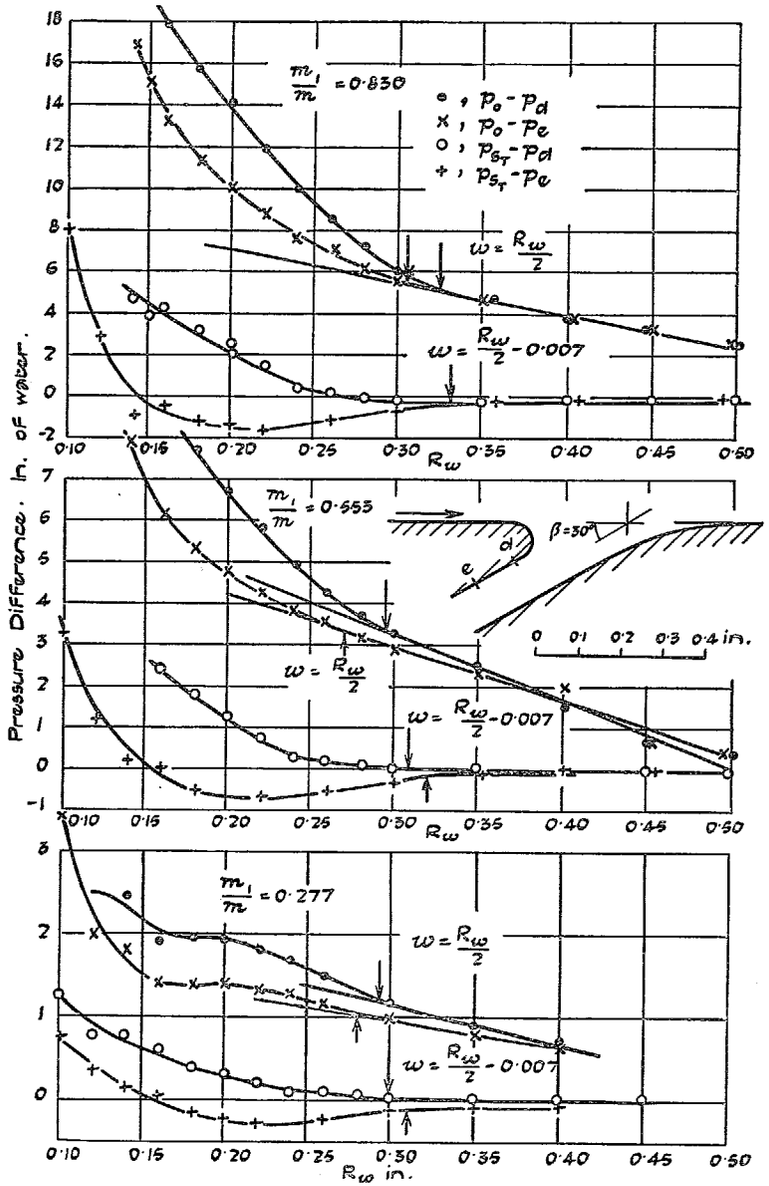


FIG. 18. Turbulent Flow. $U_s = 83{\cdot}6$ ft./sec.
$\beta = 30$ deg. $r_1 = 0{\cdot}045$ in.

[*Note.*—Figs. 19 to 21 are on page 27].

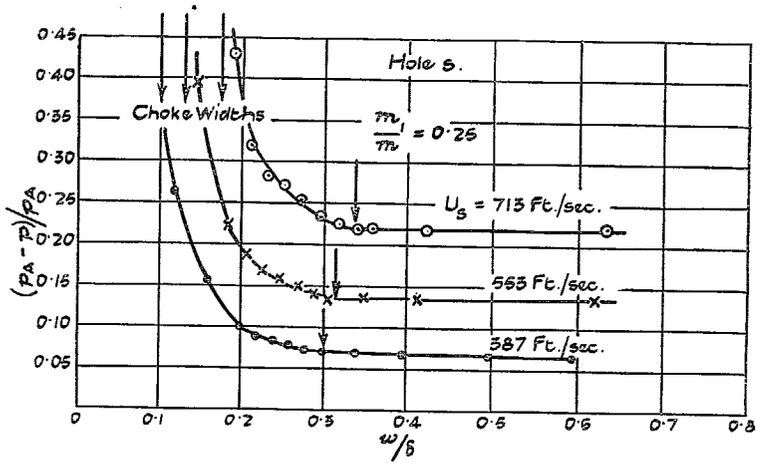


FIG. 22. Turbulent Boundary Layer. Compressible Flow.
$\beta = 150$ deg., $r_1 = 0{\cdot}6$ in., $r_2 = 0{\cdot}065$ in.

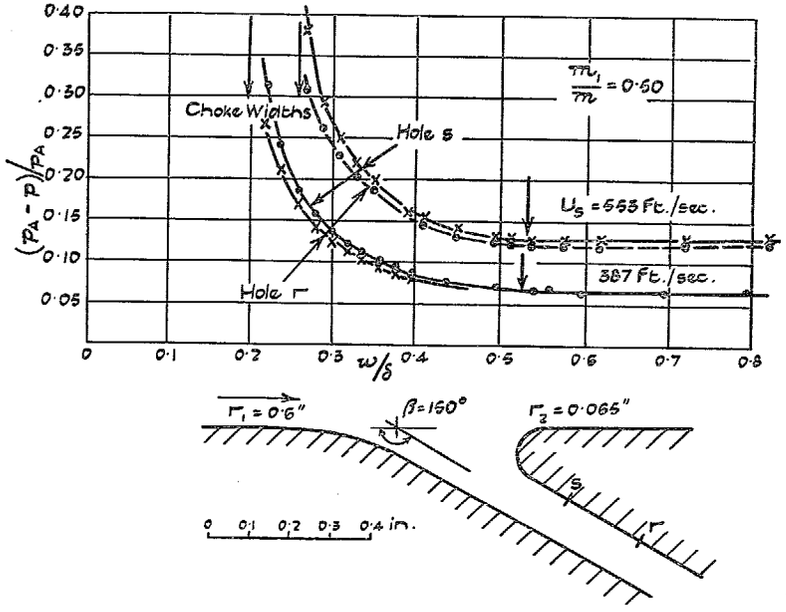


FIG. 23. Turbulent Boundary Layer. Compressible Flow.
$\beta = 150$ deg., $r_1 = 0{\cdot}6$ in., $r_2 = 0{\cdot}065$ in.

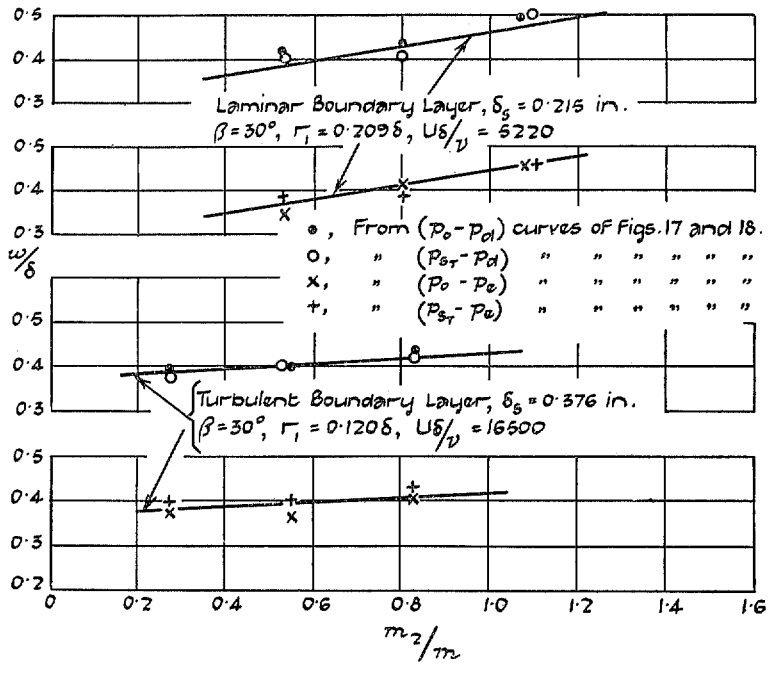


FIG. 19.

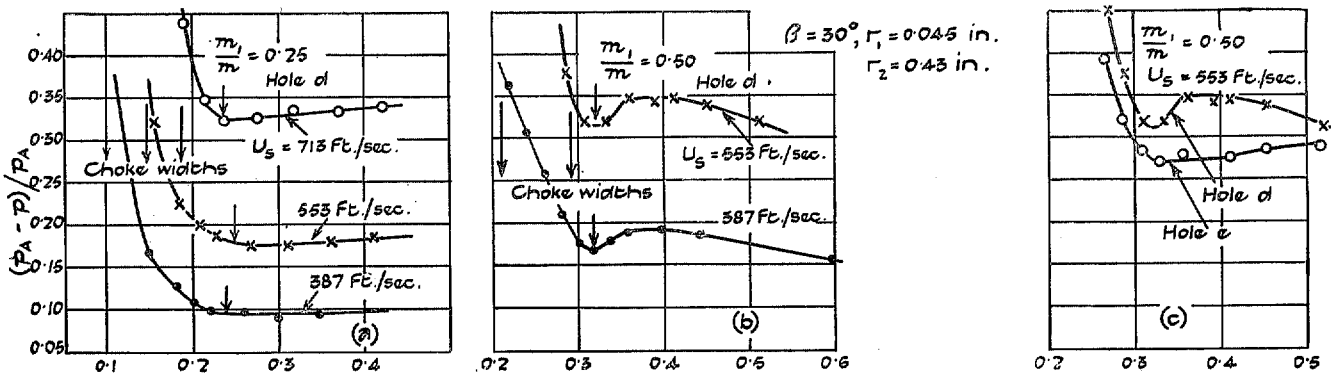


FIG. 20. Turbulent Boundary Layer. Compressible Flow.

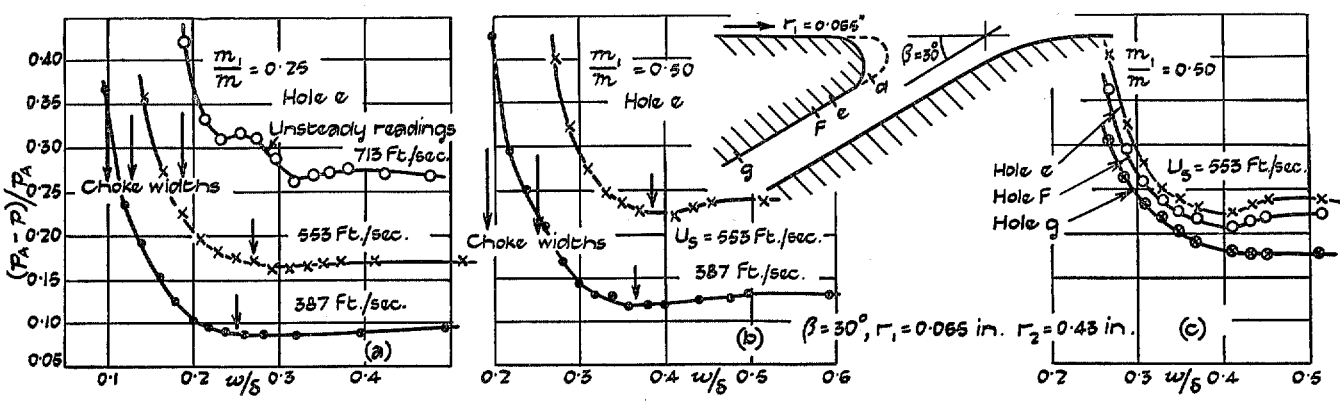


FIG. 21. Turbulent Boundary Layer. Compressible Flow.

(*Note.*—Figs. 22 and 23 are on page 26.)

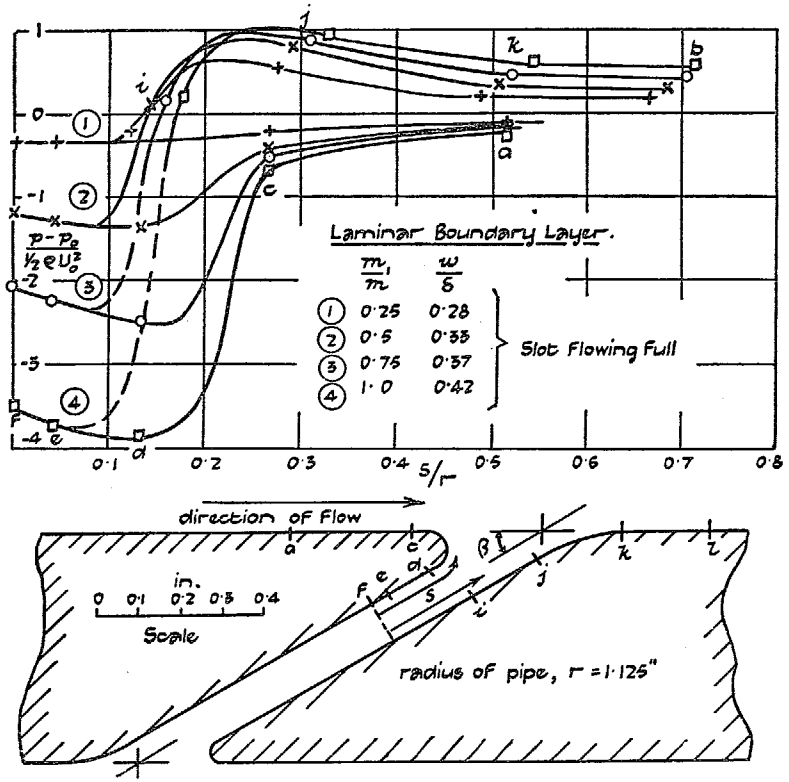


Section of Slot.

FIG. 24.

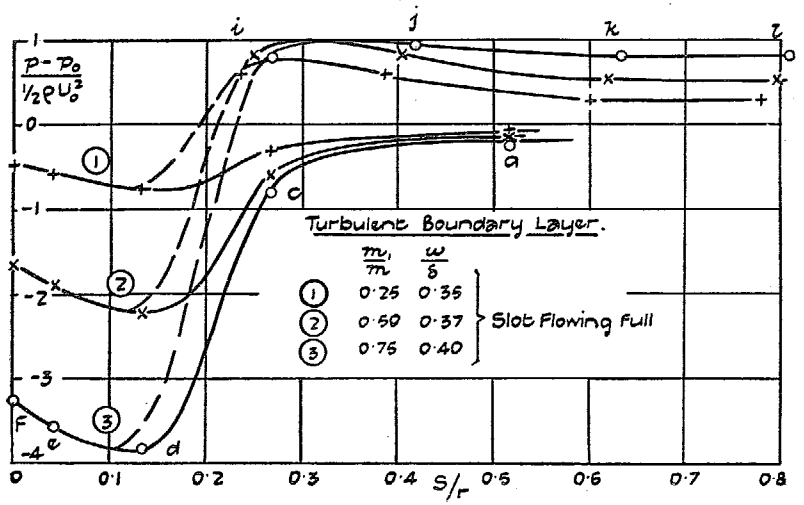


FIG. 25. Incompressible Flow. $\beta = 30$ deg., $r_1 = 0 \cdot 045$ in., $r_2 = 0 \cdot 43$ in.

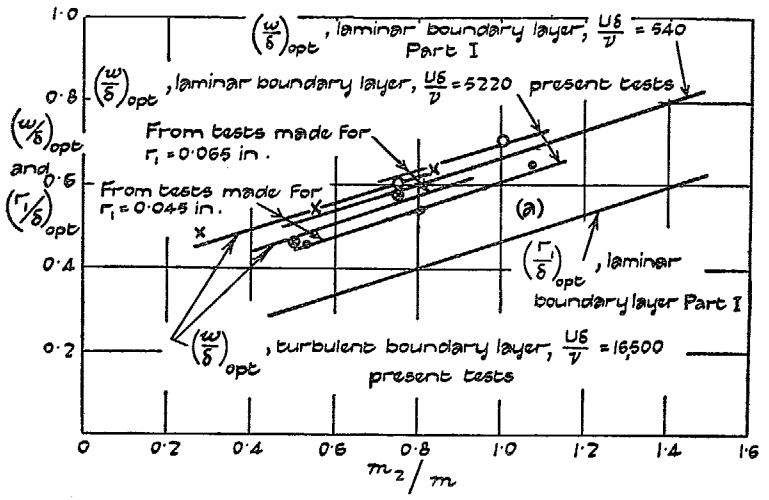


FIG. 26. Incompressible Flow, $\beta = 30$ deg.

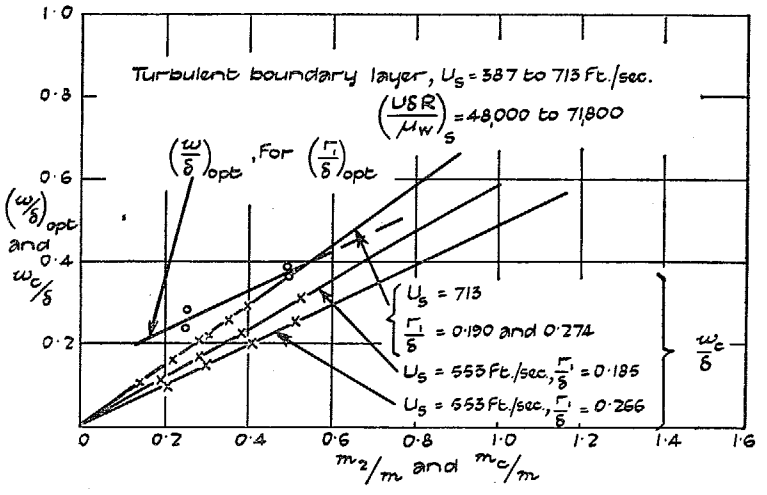


FIG. 27 Compressible Flow, $\beta = 30$ deg.

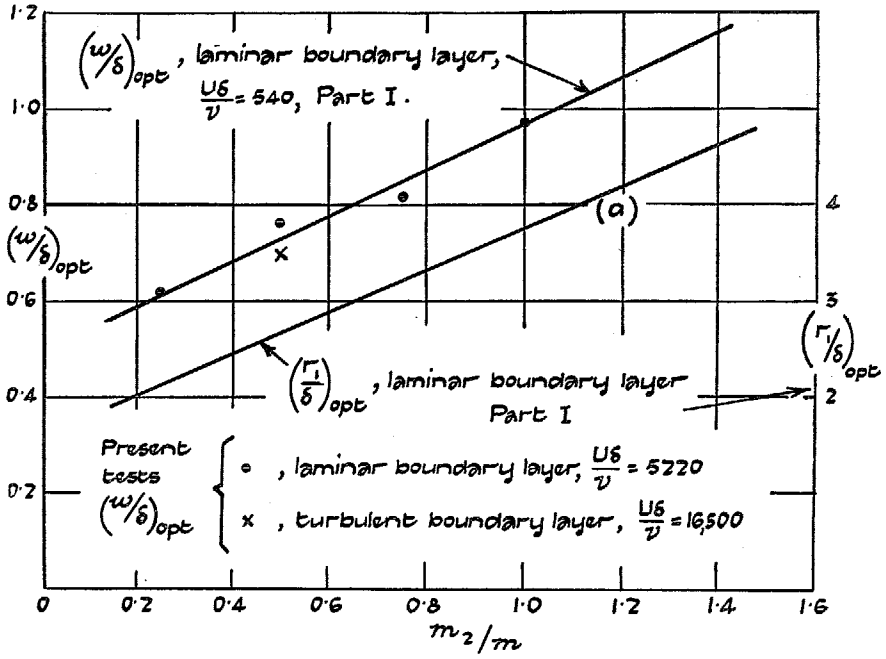


FIG. 28. Incompressible Flow, $\beta = 150$ deg.

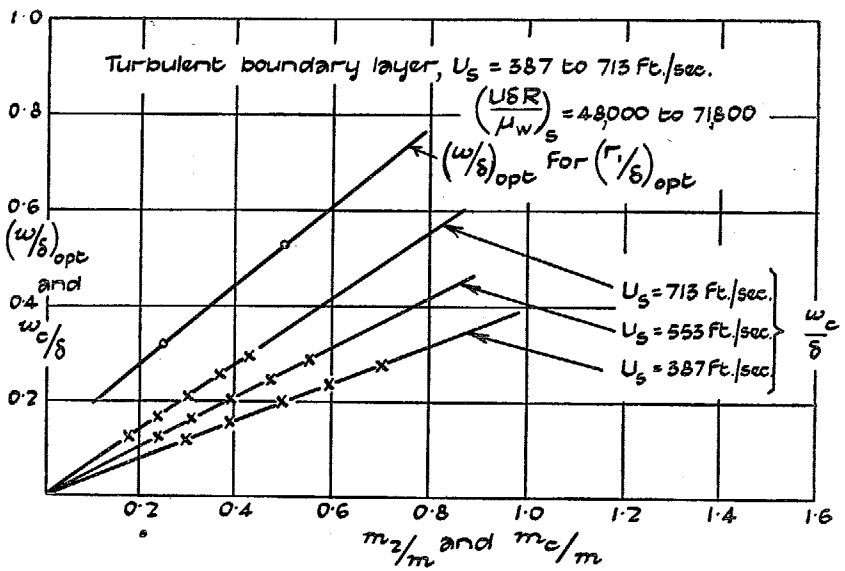


FIG. 29. Compressible Flow, $\beta = 150$ deg.

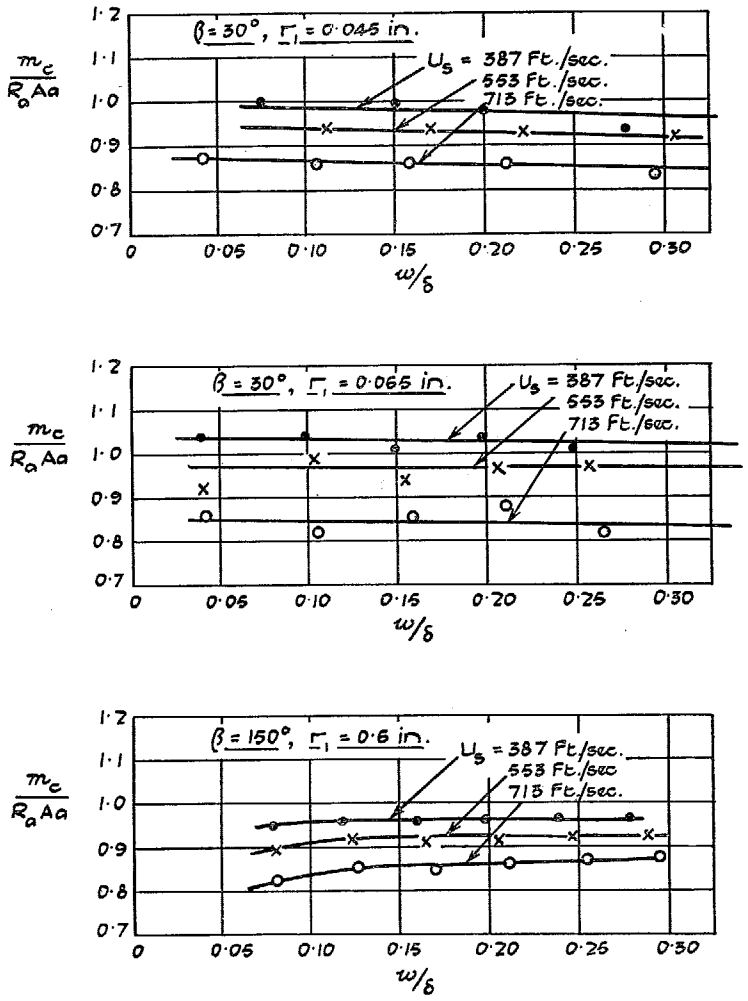


FIG. 30. Choke Conditions.

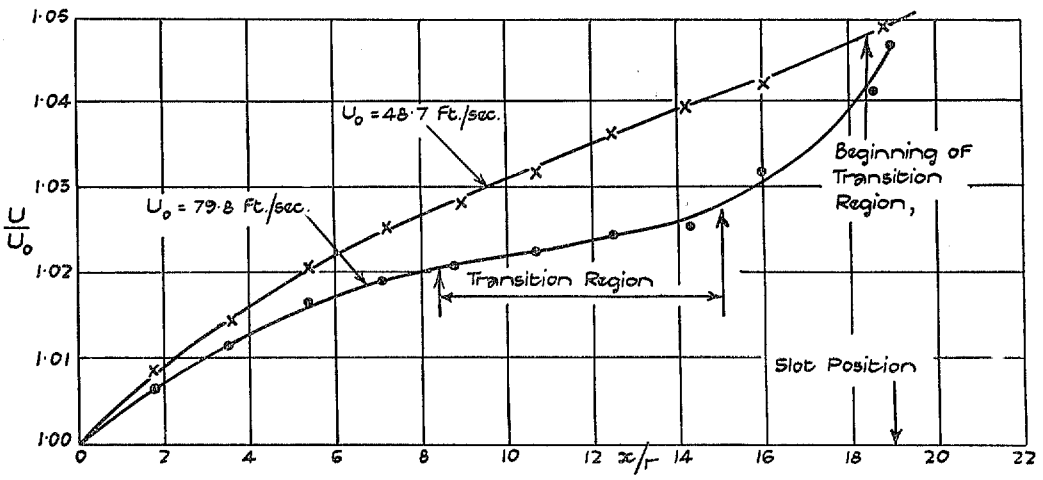


FIG. 31. Distribution of $U/U_0$ down Pipe.

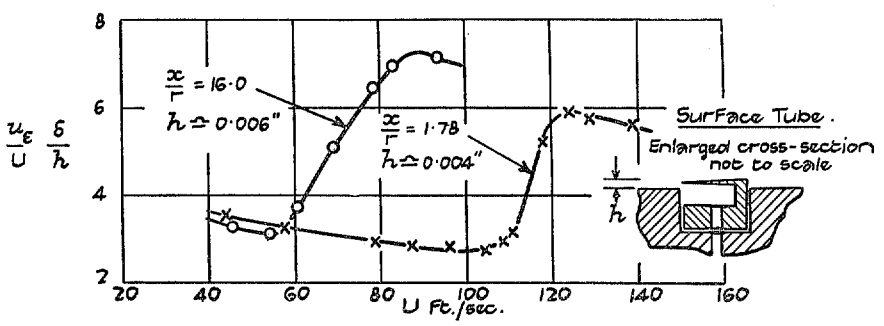


FIG. 32. Surface Tube Measurements.

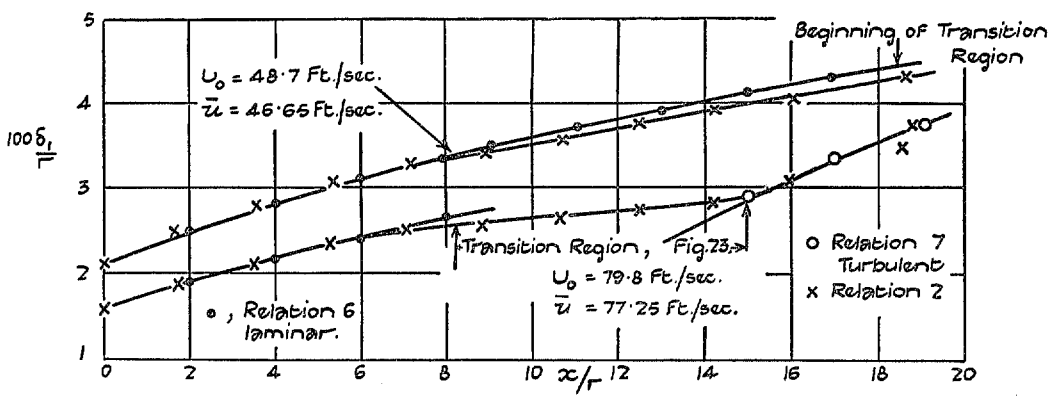


FIG. 33.

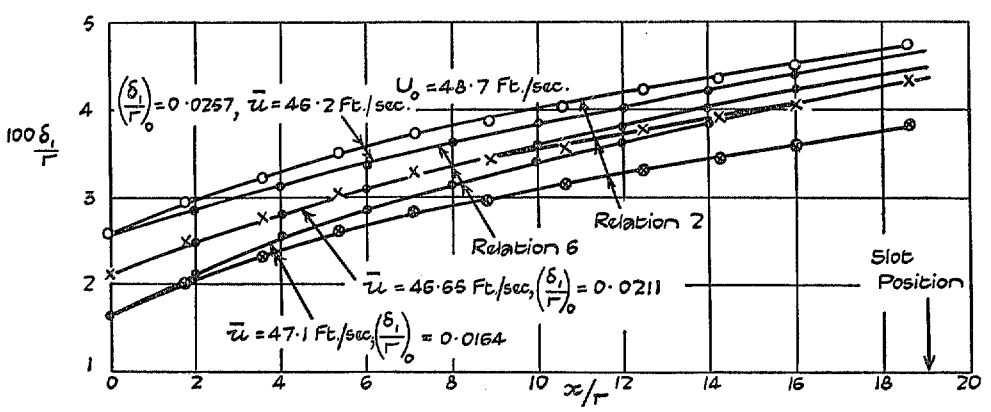


FIG. 34.

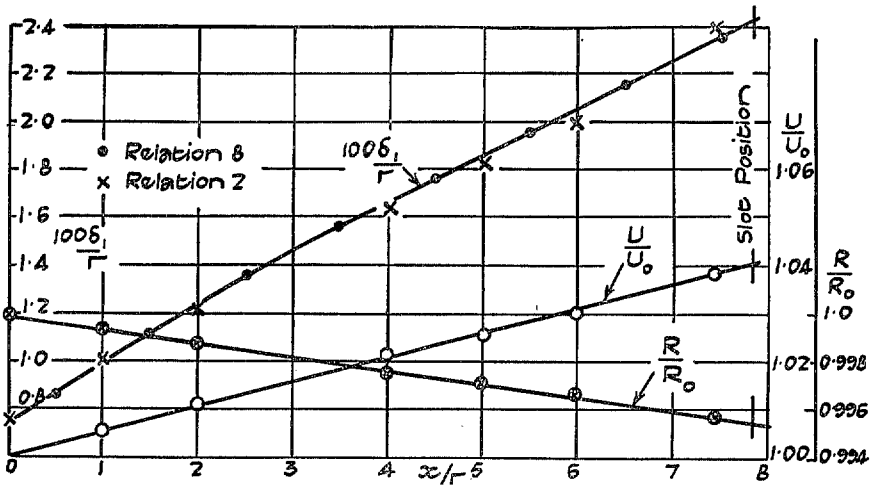


$U_0 = 372$ ft./sec. $M_0 = 0{\cdot}337$.

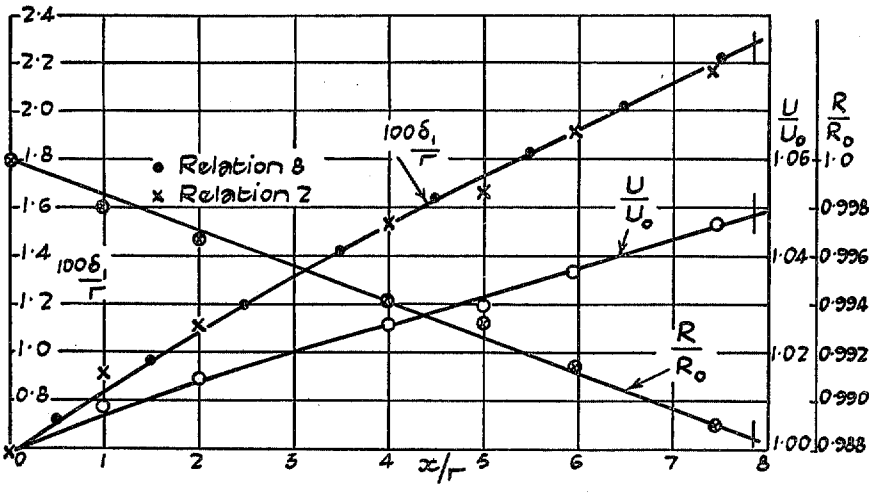


$U_0 = 527$ ft./sec. $M_0 = 0{\cdot}487$.

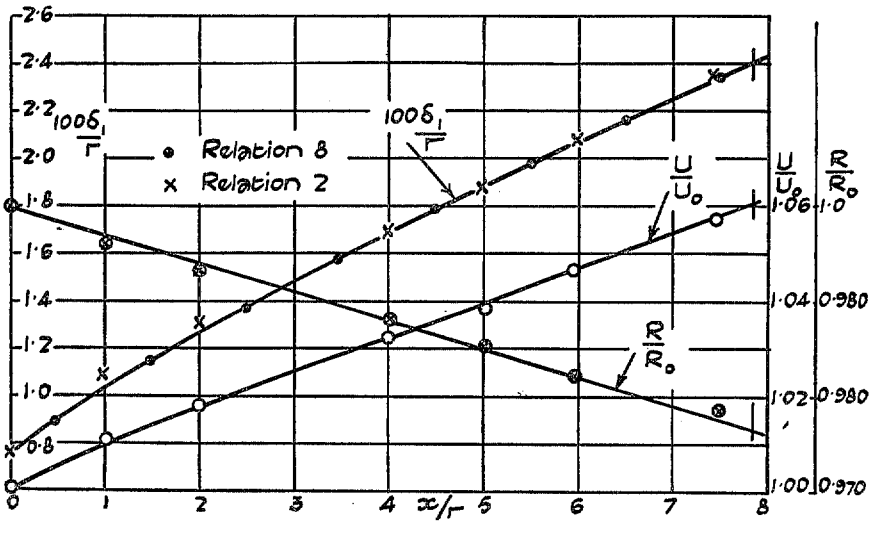


$U_0 = 673$ ft./sec. $M_0 = 0{\cdot}628$.

FIG. 35.

(77256) Wt. 10/7116 9/47 Hw. G.377/1

# Publications of the Aeronautical Research Committee

TECHNICAL REPORTS OF THE AERONAUTICAL RESEARCH COMMITTEE—

1934-35 Vol. I. Aerodynamics. 40*s.* (40*s.* 8*d.*)
Vol. II. Seaplanes, Structures, Engines, Materials, etc. 40*s.* (40*s.* 8*d.*)

1935-36 Vol. I. Aerodynamics. 30*s.* (30*s.* 7*d.*)
Vol. II. Structures, Flutter, Engines, Seaplanes, etc. 30*s.* (30*s.* 7*d.*)

1936 Vol. I. Aerodynamics General, Performance, Airscrews, Flutter and Spinning. 40*s.* (40*s.* 9*d.*)
Vol. II. Stability and Control, Structures, Seaplanes, Engines, etc. 50*s.* (50*s.* 10*d.*)

1937 Vol. I. Aerodynamics General, Performance, Airscrews, Flutter and Spinning. 40*s.* (40*s.* 9*d.*)
Vol. II. Stability and Control, Structures, Seaplanes, Engines, etc. 60*s.* (61*s.*)

ANNUAL REPORTS OF THE AERONAUTICAL RESEARCH COMMITTEE—

1933-34 1*s.* 6*d.* (1*s.* 8*d.*)
1934-35 1*s.* 6*d.* (1*s.* 8*d.*)
April 1, 1935 to December 31, 1936. 4*s.* (4*s.* 4*d.*)
1937 2*s.* (2*s.* 2*d.*)
1938 1*s.* 6*d.* (1*s.* 8*d.*)

INDEXES TO THE TECHNICAL REPORTS OF THE ADVISORY COMMITTEE ON AERONAUTICS—

December 1, 1936 — June 30, 1939
Reports & Memoranda No. 1850. 1*s.* 3*d.* (1*s.* 5*d.*)

July 1, 1939 — June 30, 1945
Reports & Memoranda No. 1950. 1*s.* (1*s.* 2*d.*)

*Prices in brackets include postage.*

Obtainable from

## His Majesty's Stationery Office

London W.C.2 : York House, Kingsway
[Post Orders—P.O. Box No. 569, London, S.E.1.]
Edinburgh 2: 13A Castle Street
Manchester 2: 39-41 King Street
Cardiff: 1 St. Andrew's Crescent
Belfast: 80 Chichester Street
or through any bookseller.

S.O. Code No. 23-2127